

High-Temperature Salt Pump Review and Guidelines—Phase I Report



Kevin R. Robb
Prashant K. Jain
Thomas J. Hazelwood

Approved for public release.
Distribution is unlimited.

May 2016

DOCUMENT AVAILABILITY

Reports produced after January 1, 1996, are generally available free via US Department of Energy (DOE) SciTech Connect.

Website <http://www.osti.gov/scitech/>

Reports produced before January 1, 1996, may be purchased by members of the public from the following source:

National Technical Information Service
5285 Port Royal Road
Springfield, VA 22161
Telephone 703-605-6000 (1-800-553-6847)
TDD 703-487-4639
Fax 703-605-6900
E-mail info@ntis.gov
Website <http://www.ntis.gov/help/ordermethods.aspx>

Reports are available to DOE employees, DOE contractors, Energy Technology Data Exchange representatives, and International Nuclear Information System representatives from the following source:

Office of Scientific and Technical Information
PO Box 62
Oak Ridge, TN 37831
Telephone 865-576-8401
Fax 865-576-5728
E-mail reports@osti.gov
Website <http://www.osti.gov/contact.html>

This report was prepared as an account of work sponsored by an agency of the United States Government. Neither the United States Government nor any agency thereof, nor any of their employees, makes any warranty, express or implied, or assumes any legal liability or responsibility for the accuracy, completeness, or usefulness of any information, apparatus, product, or process disclosed, or represents that its use would not infringe privately owned rights. Reference herein to any specific commercial product, process, or service by trade name, trademark, manufacturer, or otherwise, does not necessarily constitute or imply its endorsement, recommendation, or favoring by the United States Government or any agency thereof. The views and opinions of authors expressed herein do not necessarily state or reflect those of the United States Government or any agency thereof.

Reactor and Nuclear Systems Division

**HIGH-TEMPERATURE SALT PUMP REVIEW AND GUIDELINES—PHASE I
REPORT**

Kevin R. Robb
Prashant K. Jain
Thomas J. Hazelwood

Date Published: May 2016

Prepared by
OAK RIDGE NATIONAL LABORATORY
Oak Ridge, TN 37831-6283
managed by
UT-BATTELLE, LLC
for the
US DEPARTMENT OF ENERGY
under contract DE-AC05-00OR22725

CONTENTS

LIST OF FIGURES	v
LIST OF TABLES	vii
ACRONYMS	ix
ACKNOWLEDGMENTS	xi
ABSTRACT	xiii
1. INTRODUCTION	1
2. REVIEW OF FLUORIDE SALT PUMPS	3
2.1 PAST PUMPS DEVELOPED AND TESTED 1950–1970s	3
2.1.1 Decision to Develop a Centrifugal-type Pump with an Overhung Impeller	3
2.1.2 Overview of Fluoride-salt Centrifugal Pumps Developed	4
2.1.3 Shaft Seals	6
2.1.4 Conventional Bearings	6
2.1.5 Long-shaft Pump and Salt-wetted Bearings	7
2.1.6 Impeller and Housing	8
2.1.7 Pump Tank, Impeller Casing—Entrainment, Degassing, Level Surge, Aerosols	8
2.1.8 Radiation—Shielding, Degradation, Maintenance	9
2.1.9 Reactor Operation Experience	9
2.1.10 Development Path Summary	10
2.2 ORNL LSTL PUMP	11
3. PROPOSED PUMP TEST PLAN	15
3.1 COLD SHAKEDOWN TESTING	15
3.1.1 Test Stand Design	15
3.1.2 Proposed Tests	16
3.2 HOT TESTING	17
3.2.1 Loop Modification Design	17
3.2.2 Proposed Testing	18
4. PERFORMANCE CHARACTERISTICS OF THE LSTL PUMP MK1	21
4.1 PREDICTED HYDRAULIC PERFORMANCE	21
4.1.1 Computational Fluid Dynamics Model	21
4.1.2 Boundary Conditions for the CFD Model	23
4.1.3 Numerical Mesh for the CFD Model	24
4.1.4 Material Properties for the Molten Salt	26
4.1.5 Pseudo-Steady CFD Results	27
4.1.6 Pump Affinity Laws	33
4.1.7 Time-dependent CFD results	37
4.2 PREDICTED SHAFT VIBRATION CHARACTERISTICS	40
4.2.1 Modeling Assumptions	40
4.2.2 Calculation Input	40
4.2.3 Analysis Results	43
4.2.4 Findings and Path Forward	48
4.3 COLD SHAKEDOWN TESTING	49
4.3.1 Initial alignment	49
4.3.2 Static Vibration Data	49
4.4 FUTURE PLANS	54
5. EXAMPLE DESIGN GOALS AND REQUIREMENTS FOR A NEW LSTL-MK2 PUMP	56
5.1 DESIGN GOALS AND REQUIREMENTS	56
5.1.1 Goals	56
5.1.2 Requirements	56

6. SUMMARY.....	58
7. REFERENCES	60

LIST OF FIGURES

Figure 1. Past fluoride salt pump design space and experience base.....	5
Figure 2. Picture of LSTL pump impeller and volute.....	11
Figure 3. Picture of LSTL assembled volute.....	12
Figure 4. Picture of pump indicating accelerometer locations.....	13
Figure 5. Pump cold shakedown test stand.....	15
Figure 6. Illustration of LSTL modification for pump testing.....	18
Figure 7. A detailed CAD model for the ORNL molten salt pump assembly.....	21
Figure 8. Description for the CFD model boundary conditions.....	24
Figure 9. Free tetrahedral finite element mesh with boundary layers for the pump CFD model. This mesh results in a wall lift off (in viscous units) y^+ value of 11.1, in compliance with the specific k-e model implemented in COMSOL.....	25
Figure 10. Variation of FLiNaK salt properties with temperature.....	26
Figure 11. Typical flow streamlines as predicted by the pump CFD model.....	27
Figure 12. Pseudo-steady pressure (psi) distribution at 1,750 rpm for different outlet discharge rates.....	28
Figure 13. Pseudo-steady pressure (psi) distribution at 1,750 rpm for different outlet discharge rates.....	29
Figure 14. The locations of vertical and horizontal cut planes for visualizing CFD results.....	30
Figure 15. Velocity (m/s) and pressure (psi) contours for different discharge rates, plotted on a vertical cut plane through the pump operating at 1,750 rpm.....	31
Figure 16. Velocity (m/s) and pressure (psi) contours for different discharge rates, plotted on a horizontal cut plane through the pump operating at 1,750 rpm.....	32
Figure 17. Pump performance as predicted by the CFD model at 1750 rpm.....	33
Figure 18. Head flow performance curves for the ORNL pump—as predicted by the CFD model.....	35
Figure 19. Power imparted to the liquid by the pump for different operating speeds, as predicted by the CFD model.....	36
Figure 20. Pump efficiency results for different operating speeds—as predicted by the CFD model.....	37
Figure 21. Time-dependent CFD model results at 1,750 rpm for the pump discharge pressure and total head for three different discharge rates. The asterisks (*) indicate their corresponding steady state values as obtained from separate frozen rotor simulations.....	38
Figure 22. Time-dependent pressure (psi) variation on the horizontal cut plane at different times: (a) $t = 2$ ms, (b) $t = 10$ ms, and (c) $t = 30$ ms (pump operating speed = 1,750 rpm and discharge velocity = 3 m/s).....	39
Figure 23. Three-dimensional shaft model mesh.....	41
Figure 24. Three-dimensional geometry.....	42
Figure 25. Three-dimensional support.....	42
Figure 26. Displacement mode 1: (A) beam model, (B) 3-D model.....	44
Figure 27. Displacement mode 2: (A) beam model, (B) 3-D model.....	44
Figure 28. Displacement mode 3: (A) beam model, (B) 3-D model.....	45
Figure 29. Displacement mode 4: (A) beam model, (B) 3-D model.....	45
Figure 30. Displacement mode 5: (A) beam model, (B) 3-D model.....	46
Figure 31. Displacement mode 6: (A) beam model, (B) 3-D model.....	46
Figure 32. Displacement mode 7: (A) beam model, (B) 3-D model.....	47
Figure 33. Displacement mode 8: (A) beam model, (B) 3-D model.....	47
Figure 34. Displacement mode 9: (A) beam model, (B) 3-D model.....	48
Figure 35. Displacement mode 10: (A) beam model, (B) 3-D model.....	48
Figure 36. Impact test frequency response function data.....	52

Figure 37. Operational deflection shape at 7 Hz.....	53
Figure 38. Operational deflection shape at 25 Hz.....	53
Figure 39. Operational deflection shape at 44 Hz.....	53
Figure 40. Operational deflection shape at 55 Hz.....	53
Figure 41. Operational deflection shape at 115 Hz.....	54
Figure 42. Operational deflection shape at 162 Hz.....	54

LIST OF TABLES

Table 1. Summary of pumps developed during the ANP and MSR programs	4
Table 2. CFD boundary conditions	23
Table 3. COMSOL CFD mesh setup	24
Table 4. Inconel 600 mechanical properties for vibration analyses	40
Table 5. Natural frequencies	43
Table 6. Impact test software setup.....	50
Table 7. Impact test excitation locations.....	50
Table 8. Frequency response from impact test.....	50

ACRONYMS

3-D	three-dimensional
ANP	Aircraft Nuclear Propulsion
ARE	Aircraft Reactor Experiment
ART	Aircraft Reactor Test
CFD	computational fluid dynamics
CRADA	Cooperative Research and Development Agreement
FHR	fluoride salt-cooled high-temperature reactor
FRF	frequency response functions
LSTL	liquid salt test loop
MSR	Molten Salt Reactor
MSRE	Molten Salt Reactor Experiment
ORNL	Oak Ridge National Laboratory
SINAP	Shanghai Institute of Applied Physics
SS	stainless steel

ACKNOWLEDGMENTS

This work was performed as part of the cooperative research and development agreement NFE-13-04825 between the US Department of Energy's Oak Ridge National Laboratory and the Chinese Academy of Sciences' Shanghai Institute of Applied Physics.

Jerry Terrell and Kurt Smith provided valuable assistance in the design and drafting of the loop modifications and cold shakedown test stand. Blake Van Hoy and Claire Luttrell assisted the vibration modeling and testing. Dennis Heatherly, Doug Sparks, Graydon Yoder Jr., and Bob Sitterson developed the original design and assembled the salt loop pump.

ABSTRACT

Fluoride salt-cooled high-temperature reactor (FHR) concepts include pumps for forced circulation of the primary and secondary coolants. As part of a cooperative research and development agreement between the Shanghai Institute of Applied Physics and the Oak Ridge National Laboratory (ORNL), a research project was initiated to aid in the development of pumps for high-temperature salts. The objectives of the task included characterization of the behavior of an existing ORNL LSTL pump; design and test a modified impeller and volute for improved pump characteristics; and finally, provide lessons learned, recommendations, and guidelines for salt pump development and design. The pump included on the liquid salt test loop (LSTL) at ORNL served as a case study. This report summarizes the progress to date.

The report is organized as follows. First, there is a review, focused on pumps, of the significant amount of work on salts at ORNL during the 1950s–1970s. The existing pump on the LSTL is then described. Plans for hot and cold testing of the pump are then discussed, including the design for a cold shakedown test stand and the required LSTL modifications for hot testing. Initial hydraulic and vibration modeling of the LSTL pump is documented. Later, test data from the LSTL will be used to validate the modeling approaches, which could then be used for future pump design efforts. Some initial insights and test data from the pump are then provided. Finally, some preliminary design goals and requirements for a future LSTL pump are provided as examples of salt pump design considerations.

1. INTRODUCTION

Pump design is an important consideration in the design of a forced-circulation system. Most postulated nuclear or solar thermal salt systems rely on forced circulation to transfer heat from the source to the end process (power cycle or heat application). In electrochemical processes, pumps are primarily used for transferring the working fluid from one location to another. In addition, pumps are used in forced-circulation loops for the testing of components (i.e., heat exchangers), material corrosion, and salt chemistry. The large heat capacity of the salt requires smaller pumps compared with those for other working fluids, such as large compressors for gas. However, the salt pumps themselves, their operation cost, maintenance, and reliability, are considerations that affect system economics. A number of other considerations affected by pumps include possible bubble entrainment, seal leakage, and gas free space dynamics, as well as transient spin up/down time, seismic performance, and so on. Finally, although next-generation nuclear systems may not rely on the pumps for ultimate heat removal during an accident, some safety considerations with respect to pump performance remain.

The liquid salt test loop (LSTL) is a high-temperature fluoride-salt forced-circulation loop developed at Oak Ridge National Laboratory (ORNL) [1, 2]. To provide forced circulation, the LSTL includes a centrifugal pump with an overhung impeller. Research and development on fluoride salt-cooled high-temperature reactors is ongoing as part of a Cooperative Research and Development Agreement (CRADA No. NFE-13-04825) between the Shanghai Institute of Applied Physics (SINAP) under the auspices of the Chinese Academy of Sciences, and ORNL under the auspices of the US Department of Energy. Under this CRADA, a task focused on salt pumps was defined with the objectives to characterize the behavior of an existing ORNL LSTL pump; design and test a modified impeller and volute for improved pump characteristics; and finally, provide lessons learned, recommendations, and guidelines for salt pump development and design.

This report documents the efforts and accomplishments to date on this task. Future efforts will expand upon the work documented in this report. The following are some of the key accomplishments:

- Review of past pump development efforts at ORNL, Section 2.1
- Addition of accelerometers to the LSTL pump for future data acquisition, Section 2.2
- Development of a cold test stand for pump testing, Section 3.1
- Draft plans for LSTL modification for hot salt testing of the pump, Section 3.2
- Modeling and analysis of the hydraulic characteristics of the LSTL pump, Section 4.1
- Modeling and analysis of the vibration characteristics of the LSTL pump, Section 4.2
- Static vibration data for the LSTL pump, Section 4.3.2
- Draft design goals and requirements for consideration for future pumps, Section 5

2. REVIEW OF FLUORIDE SALT PUMPS

During the 1950s, 1960s, and 1970s, there was a wide range of salt pump development activities at ORNL. More recently, the LSTL, which includes a pump to circulate fluoride salts was developed at ORNL [1, 2]. This section summarizes the past development efforts and the current pump as part of the LSTL.

2.1 PAST PUMPS DEVELOPED AND TESTED 1950–1970s

The Aircraft Nuclear Propulsion (ANP) program spanned from 1951 to 1961. The goal of the program, to develop a lightweight reactor suitable to powering an aircraft, resulted in the focused development of molten salt reactors. To enable the molten salt reactor, there was a large effort in technology development, including pumps for fluoride salt, sodium, and sodium-potassium eutectic (NaK). The program resulted in the Aircraft Reactor Experiment (ARE) going critical in 1954 and the zero-power Pratt and Whitney Aircraft Reactor No. 1 in 1957. Plans and technology for a larger test reactor, the Aircraft Reactor Test (ART), were under development at the time of project cancellation.

Building on the ANP program, the Molten Salt Reactor (MSR) program was initiated at ORNL in 1957 with a focus on terrestrial power reactors using fluoride-based salts. The effort was initially cancelled and reinstated in 1973 and final program cancellation occurred in 1976. The program resulted in the Molten Salt Reactor Experiment (MSRE) going critical in 1965. After the MSRE, technology was being developed for larger molten-salt reactors at the time of project cancellation.

During the same period, considerable work was also being performed on other high-temperature pumps, such as those for sodium. This report focuses specifically on the pump development and experience for fluoride-salt pumps. The following sections discuss the pumps developed, the development of key pump components, experience, and issues encountered.

2.1.1 Decision to Develop a Centrifugal-type Pump with an Overhung Impeller

During the ANP program, centrifugal, canned rotor, and electromagnetic pumps were developed and tested. Canned rotor pumps were tested in NaK, one at a maximum temperature of 1,085°F [3]. However, the thin casing of the canned rotor pump was viewed as a potential hazard, and the size of the pump and associated electrical equipment was not acceptable to the ANP program [4]. In addition, canned-rotor pumps were not available at that time for the required operating temperatures [4]. Electromagnetic pumps were tested in sodium, one at a maximum temperature of 1,500°F [3]. However, the electromagnetic pumps, which are not suitable for fluoride salts, were too large in size and weight (including the required electrical equipment) with respect to the ANP program application [4]. Owing to those reasons and the better efficiency of centrifugal pumps, the ANP and MSR programs primarily focused on the development of centrifugal pumps.

Two types of centrifugal pumps are defined (long-shaft, short-shaft) based on their bearing configuration. Long-shaft pumps are supported with bearings both above and below the impeller. Short-shaft pumps have bearings only on one side of the impeller outside the shaft seal, so the shaft between the seal and the impeller is cantilevered. The challenges associated with salt-wetted bearings, using the materials of the time, resulted in most of the development and testing being focused on short-shaft pumps. The limited work on long-shaft pumps and salt-wetted journal bearings is discussed Section 2.1.5.

2.1.2 Overview of Fluoride-salt Centrifugal Pumps Developed

A large number of pumps were developed and tested as part of the ANP and MSR programs. Table 1 summarizes many of the pumps that were developed, the general design point operating conditions, and the number of hours for which they were tested. Excluded from the table are a number of pumps that were developed and tested that led to the pumps listed in Table 1. Also excluded are pumps that were tested just in sodium or NaK.

As is seen in Table 1, the pumps cover a wide range of operating conditions. The total hours of run-time experience were also extensive, totaling over 96 years. Figure 1 is an illustration of the design space and operating experience of the past pumps based on the information in Table 1; circle size in Figure 1 is proportional to the pump operation time.

Table 1. Summary of pumps developed during the ANP and MSR programs

Pump	Fluid ^a	At design point			Temp. (°C)	No. built	Total hours	Ref.
		Head (m)	Flow (m ³ /h)	Speed (rpm)				
LFB	MS, Na, NaK	28	1.1	6,000	593–760	46	451,000	5
LFB	MS		0.9	5,000	510		10,000	6
DANA	MS, Na, NaK	91	34.1	3,750	538–816	10	57,000	5
DAC	MS	15	13.6	1,450	538–760	3	4,000	5
In-pile Loop (LFA)	MS	3	0.2	3,000		8	14,000	5
MF	MS, NaK	15	159	3,000	593–816	3	41,000	5
PKA	MS, NaK	122	85.1	3,550	371–816	2	19,000	5
PKP	MS, NaK	116	341	3,500	371–816	4	40,000	5
PKP	MS		182	1,800	482–691		1,1567	7
MSRE Prototype–Fuel	MS	15	272	1,150	593–816	1	89,000	5
MSRE Test Stand–Fuel	MS	15	272	1,150	593–704	2	3,300	5
MSRE Operation–Fuel	MS	15	272	1,175	538–663 ^b		21,788 ^c	5
MSRE Test Stand–Cool.	MS	30	193	1,750	593–704	2	1,600	5
MSRE Operation–Coolant	MS	24	182	1,775	538–691 ^b		2,6076 ^c	5
MSRE Mark-2–Fuel	MS	16	306	1,165	549–732	1	16,680	^d
ALPHA	MS	76	6.8	6,000	454	1 ^e	6,800 ^f	8
ALPHA	MS	76	6.8	6,000	566–727		12,000 ^g	8
Long-shaft pump ^h	MS	15	59	1,300	593–732	1	13,616	5

^a MS: molten fluoride salt

^b Operated primarily at 1200°F (649°C)

^c Time above 1000°F (538°C) in salt

^d Multiple program quarterly reports

^e Additional pumps fabricated but not used

^f Operated at 4 gpm, 4,800 rpm

^g Operated at 3.1 gpm, 4,000 rpm

^h Only long-shaft type pump extensively tested

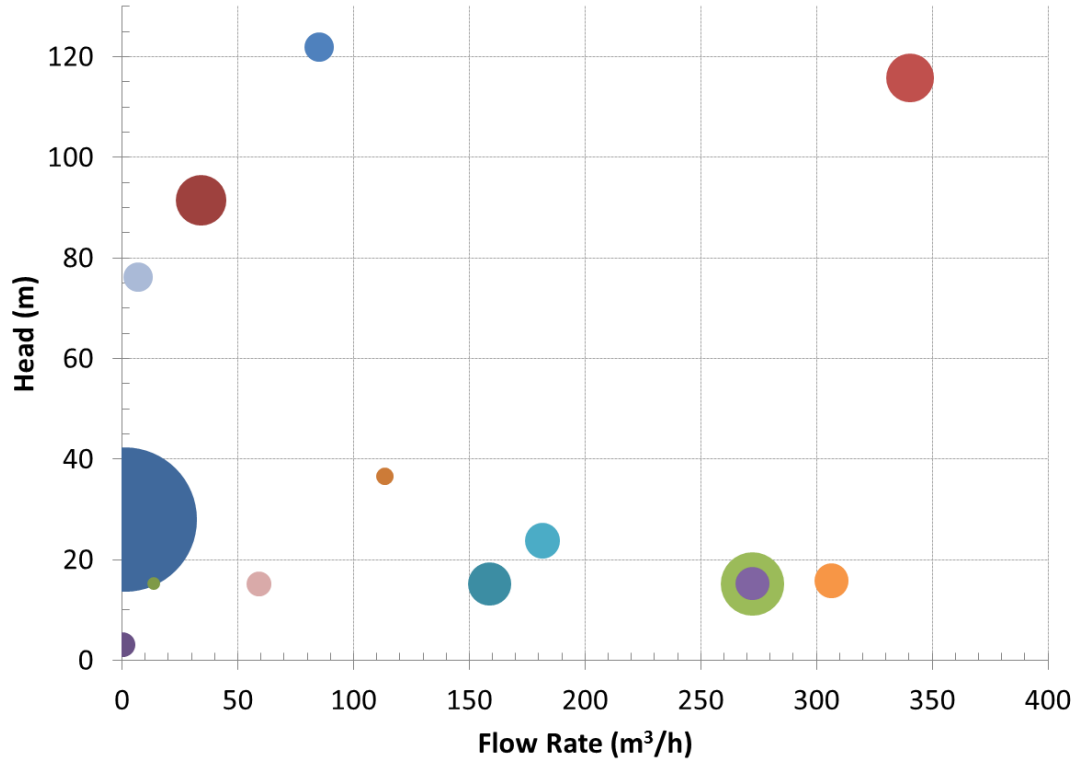


Figure 1. Past fluoride salt pump design space and experience base.

The LFB, DANA, and DAC centrifugal pump models were developed leading up to the ARE. The LFB pump was a general purpose pump used in forced-circulation loops for component and/or materials testing. The DAC model was developed as the ARE fuel pump, and the DANA was developed as the ARE sodium pump. Earlier, several additional pumps were designed and tested leading up to the LFB, DANA, and DAC pumps [3].

For the ART, the MF model fuel pump, MN model sodium pump, PK-P model primary NaK pump, and PK-A model auxiliary NaK pump were developed. The MN pump was tested only in sodium and is not included in Table 1. Although the ART was never constructed, the pumps were developed, tested, and used for other testing purposes.

For the MSRE, the Mark-1 and Mark-2 model pumps were developed and operated [9, 10]. The PKP pump served as the predecessor to the MSRE pumps. Toward the end of the MSR program, the ALPHA model pump [8] was developed as a higher-capacity general purpose pump.

The development and testing of these pumps, with a particular focus on seals, are well summarized by Farris [3] for the time period July 1950–January 1954. The development is also briefly summarized in refs. [4, 5, 11, 12] and in the many ANP and MSR program topical and progress reports. The following sections discuss key pump components, their design and operating experience, and other related development activities. The discussion specifically focuses on pumps for fluoride salt.

2.1.3 Shaft Seals

Shaft seals were identified during the ANP program as the principle design challenge with respect to high-temperature pumps. A number of seal variants were investigated, including mechanical and frozen seals.

Stuffing box type seals, using various packing materials, were investigated [4]. As recorded in Tunnel [9], 26 permeation tests (1,500°F salt) and 26 tests with a rotating shaft (1,050–1,500°F salt) were performed, primarily in NaF-ZrF₄-UF₄ salt. Seals made of graphite or graphite with additives were the best performers. However, there was a difficulty with retaining the materials in the stuffing boxes. Also, the seals were more successful when they were at temperatures lower than the salt melting point. At the lower temperatures, the packed seals acted as frozen-type seals. Frozen seals have higher power demands and can lead to severe scoring of the shaft. Other stuffing materials, such as boron nitride or metallic-based materials, presented issues of either poor lubrication and/or scoring of the shaft. A solid sleeve-type packing was developed and designed for a specific operating temperature. The seal worked well at a temperature above the salt melting point; however, the seal leakage rate was temperature dependent (because of differential degrees of thermal expansion). In general, some seal configurations showed promise during shorter-term testing; however, shaft scoring or gas leakage rates were unacceptable [4] and their development was not further pursued.

The DANA and DAC model pumps used in the ARE (and the DA, LF, and DAB development pumps) used oil-cooled rotary face gas seals. The materials hardened tool steel, Graphitar® carbon-graphite, and silver-impregnated graphite were investigated. Dry running of the silver-impregnated material was tested with the LF pump but proved unsuccessful. Dry running of another rotary face seal with an Allis-Chalmers pump resulted in chattering and was also unsuccessful. Thus, the seals were oil lubricated. The primary seal for the DAC and DANA pumps used silver-impregnated graphite between optically flat hardened steel surfaces [4]. Through development, oil leakage of 2–5 cc/day and gas leakage <15 cc/day across the seal were attained.

A number of frozen seal configurations were investigated [3]. In a frozen seal, the shaft rotation heats and melts a small amount of the material next to the rotating component, and that fluid acts as the seal and lubricant. Frozen seals for sodium pumps were found to be feasible. However, the use of a fluoride salt frozen seal was found to require precise temperature control, was difficult to start, required excessive power, and could result in severe scoring of the shaft. Another frozen seal using lead was investigated. The seal relied on the density-driven segregation of the lead from the salt. However, in operation, lead was found to be mixed into the fluoride salt, and further development was not pursued.

Combined packed-frozen seals were investigated [3]. However, issues were encountered with the seals similar to the issues with the noncombined packed seals and frozen fluoride salt seals.

A unique “centrifugal seal” was investigated in which the impeller forces the salt outward toward the walls, leaving only an annular ring of gas around the penetration in the housing for the shaft [3]. The pump was operated successfully in different orientations. However, it had to be started and stopped in the vertical orientation. Also, there was little volume available in the tank to accommodate variations in coolant level or gas pressure.

2.1.4 Conventional Bearings

All of the pumps used oil-lubricated and -cooled bearings located away from (generally above) the salt (except in the tests noted in Section 2.1.5). Attention to tolerances and mountings was required, but the tests followed general industrial practices [3]. Shaft seals were required to remove oil from the shaft due

to leakage from the bearing housings. The DANA and DAC pumps, for example, used conventional ground bearings [4]. A pair of angular ball bearings were used on top for the thrust load, and a single radial ball bearing was used at the lower end. The MSRE Mk-1 fuel pump used four sets of ball bearings, two on the top and two on the bottom, and operated at approximately 150°F [10]. The top bearings were angled to absorb radial and thrust loads. The bottom bearings were also angular and designed to absorb radial loads and provide additional stiffness for the shaft. The bearings had a predicted life expectancy of 300,000–500,000 h.

2.1.5 Long-shaft Pump and Salt-wetted Bearings

Testing of materials in sliding contact and wetted by a fluoride salt (50 NaF-46 ZrF₄-4 UF mol %) was conducted early during the ANP program [13]. The tests were conducted at 1,200°F. First, candidate materials underwent static corrosion testing in fluoride salts for 100 h. From this group, 36 combinations of 10 materials were selected and tested. The specimens consisted of a spinning flat round disk held against a stationary pin. A 10 lb load pushed the disk into contact with the end of the stationary pin, which was cylindrical, providing for a line contact at a 15,000 psi Hertz stress. The disk rotated at 850 rpm, providing a mean sliding contact speed of 7.4 fps. The testing was to be first performed at 1,200°F and the materials down-selected and then further tested at 1,350°F and 1,500°F. At the end of the 1,200°F testing, six material combinations were considered suitable for further higher-temperature testing: Kennametal 151A (70 TiC-20 Ni-10 NbTiTaC₃) in contact with Adamas A (94 WC-6 CO), Norbide B₄C, Caboloy 608 (83 Cr₃C₂-2 WC-15 Ni), Kennametal 151A, high-density graphite, and Adamas A in contact with Kennametal 138A (65 TiC-20 Co-15 NbTiTaC₃). Unfortunately, testing was halted after the 1,200°F tests because of project prioritization within the ANP program.

Building on the salt-wetted sliding-contact material testing performed during the ANP program [13], salt-wetted journal bearings were investigated [5, 14] during the MSR program. First, a dedicated test stand was used to develop and test the bearings [14]. All the bearings were constructed of INOR-8 (a nickel-molybdenum alloy) and were for 3 in. diameter shafts. Carburized INOR-8 was found to perform better than the plain alloy. Axial and helical groove configurations were investigated. Twenty-two tests performed in an LiF-BeF₂-UF₄ (62-37-1 mol %) salt, covering temperatures of 1,200–1,500°F (primarily 1,200°F), speeds of 600–2,700 rpm (primarily 1,200 rpm), and radial loads of 10–500 lb (primarily 200 lb) are reported in Smith. [14]. For the helical groove configuration, a few more tests were conducted comprising several hundred hours of testing and a couple hundred restarts.

Candidate bearings were fitted to a long-shafted pump and tested [5, 14]. Testing included over 567 days of run time under a range of conditions [5]. A variety of issues were encountered and overcome during testing. Some issues were not related to the bearing; some were related to the bearing mounting and others to the bearing design (coolant flow, rubbing). The benefits that other materials (carbides) could provide were recognized [14]; however, it was also acknowledged that challenges with respect to differential thermal expansion would have to be addressed.

After relatively successful testing of the bearings, plans were developed for salt-cooled bearings to be considered for use in the reactor designs after the MSRE (i.e., pumps for the molten salt breeder reactor project). However, the development effort was curtailed soon after because of the decision to go with short-shaft pump designs. Continued materials development was for application in smaller auxiliary pumps. Although plans for dynamic testing were developed, the bearing research and development appears to have ended before the tests were performed.

2.1.6 Impeller and Housing

Details for the development of pump impellers are not readily available; however, the impellers are known to have been of the radial type. The pumps included a single impeller, a single volute, and single suction and discharge locations.

For the DANA and DAC pumps, the volutes and impellers were constructed as machined weldments instead of castings; they are described in Frass and Savolainen [4]. The impellers were 8.125 in. in diameter with backward-swept vanes. The impeller and housing allowed for 5/32 in. of axial clearance for differential thermal expansion. A labyrinth seal at the shaft-inlet hub interface had an approximate 0.060 in. radial clearance. The housing around the impeller is described as a volute, but details are not readily available.

Several different impellers and impeller clearances were tested with the MSRE pumps [9, 15]. During hot shakedown testing of the MSRE pumps, shaft rubbing occurred in three instances [9]. In the first instance, the radial loads on the impeller during off-design operating conditions caused the shaft to rub against and friction weld itself to the shield plug. To remedy this, the clearance between the shield plug and the shaft was increased. In the second instance, the shaft rubbed against the shaft purge gas labyrinth seal. This was attributed to a combination of shaft deflection, run-out, and assembly eccentricities. The issue was remedied by increasing the diametric clearance. In the third instance, the impeller rubbed against the volute when cooling air was blown over the top of the pump tank. The cause was attributed to slightly skewed mounting of the volute within the tank.

2.1.7 Pump Tank, Impeller Casing—Entrainment, Degassing, Level Surge, Aerosols

To remove Xe-135 from the fuel, the MSRE pump included a salt spray [9]. The salt spray was fed by a bleed from the volute discharge. Under typical operating conditions, for the 11.5 in. diameter impeller, the salt spray was 50 gpm. For an alternate 13 in. diameter impeller investigated, the flow was high—approximately 85 gpm. After the xenon entered the pump tank gas space, the purge gas, down along the shaft near the gas seal, was used to sweep the Xe-135 from the tank.

While the salt spray removed xenon, the agitation caused by the salt spray could entrain bubbles back down into the pump entrance to be circulated through the system [9]. Tests using the MSRE pump salt shakedown loop and tests on MSRE (approximately 1,150 gpm, 1,200°F) indicated the higher 85 gpm flow rate resulted in some bubble entrainment, 2–3% by volume. With the smaller-diameter impeller, with a 50 gpm salt spray, bubble entrainment was decreased to 0.1% by volume or lower. The pump flow rate and salt level in the pump tank also influenced bubble entrainment [9, 16]. The bubbles in the pump tank also affected measurement of the salt level in the tank [16].

The spray system also generated salt aerosols [16]. These aerosols would enter the off-gas lines and freeze. Eventually, the lines would become plugged, and periodic maintenance was required to keep them open.

In addition to the issues associated with the xenon removal salt spray, a few other issues were encountered related to regulation of the pump tank gas space. During hot shakedown testing of the MSRE pumps, plugging due to salt freezing on the shaft was observed to occur twice [9]. The first instance stemmed from reversal of the downward shaft purge gas. The reversal was due to the substantial gas flow used for the bubbler level gauges in the pump tank. The second instance was attributed to the entrainment of salt into the gas space and onto the shaft because of issues during the salt filling operation.

2.1.8 Radiation—Shielding, Degradation, Maintenance

Unique to molten salt reactors is that the fuel is dissolved in the salt and circulated through the system. The fission products and activated nuclides are in closer proximity to the pump components (e.g., seals, bearings, motor) than in other reactor types. Design must anticipate and limit the breakdown of electrical insulation and lubricants. The radiation field necessitates that pumps can be remotely handled and maintained. The leakage rate requirements may also be stricter than for pumps in other reactor types. Finally, heat generated on upper pump tank structures must be removed.

The fuel pump for the MSRE had an annular shield plug made of INOR-8 (Hastelloy N) approximately 8 in. thick. The plug was bolted to the bottom of the bearing housing so that it could be removed with the rotary element. Oil was used to cool the shielding block from the top [10]. The shielding helped prevent breakdown and polymerization of the lubricating oil for the seals and bearings. It also limited the possible breakdown of the motor winding insulation due to the radiation field.

For salts carrying the fuel, it was necessary to remove the heat deposited in the upper structures of the pump and tank—from beta and gamma rays from the salt and/or deposited radionuclides. For the MSRE Mark-1 fuel pump, an external flow of gas over the pump tank was applied to maintain the structure's temperature [10]. In addition, there was a backward flow along the shaft to limit the upward back diffusion of radionuclides.

Finally, to facilitate remote handling, the fuel pump for the MSRE [9] included long bolt extensions.

2.1.9 Reactor Operation Experience

The ARE operated with NaF-ZrF₄-UF₄ fuel and a sodium circuit [17]. While the reactor operated for only approximately 9 days in 1954, the fuel system was in operation for 462 h [18]. The ARE included one fuel pump (DAC model) and one sodium pump (DANA model) as well as a backup pump for each. The fuel pump was operated at 1,080 rpm, providing approximately 46 gpm at 28 ft of head [4]. The maximum steady state operation temperature of the fuel was 1,580°F with a temperature differential of 355°F between the inlet and outlet [18]. This suggests the maximum operating temperature of the fuel pump was approximately 1,225°F. Toward the end of reactor operation, the reactor power and temperature were repeatedly cycled. No damage was noted to have occurred during operation or was observed in post-disassembly inspection [11]. It is noted that there was a leak in the gas closure of the fuel pump [17] related to the vent system [18], which allowed fission gases to escape the primary system. Other than the leak, the pumps worked satisfactorily.

The next reactor using a fluoride salt (NaF-ZrF₄-UF₄) was the zero-power Pratt and Whitney Aircraft Reactor No. 1 in 1957. However, it did not include any pumps and used gas pressure for salt transfers [19].

The MSRE operated with a LiF-BeF₂-ZrF₄-UF₄ fuel salt and a LiF-BeF₂ coolant salt [20]. The reactor went critical on June 1, 1965, and shut down permanently on December 12, 1969. During that time, the fuel and coolant pump operated in salt at over 538°C (1,000°F) for 21,788 and 26,076 h, respectively. Including operation in helium, the fuel and coolant pumps operated at temperatures over 482°C (900°F) for 30,848 and 27,438 h, respectively. Some operational characteristics of interest are summarized in the following paragraphs.

During hot shakedown testing of the MSRE pumps, as well as during in-service operation of the MSRE fuel pump, lubricating oil leaked from the seal catch basin down the outside of the shield plug and into the pump tank [9]. To remedy this issue for future pumps, the connection between the shield plug and bearing

housing was redesigned, and the modification was made to the spare fuel and coolant pumps. However, the in-use fuel and coolant pumps were not modified.

Partial fouling or plugging of the off-gas lines occurred repeatedly during MSRE operation [16]. The material included salt aerosols, generated in the pump tank (see Section 2.1.7 tank discussion), which were transported through the lines and deposited on the walls. Besides salt constituents, the solid or viscous material included carbon, believed to be from the decomposition of the oil that leaked into the tanks. Maintenance was performed to un-foul the lines. After one shutdown and before the MSRE was refilled with fuel salt, a flush salt was passed through the system. During this operation, the fuel pump tank was overfilled, and some salt froze in the off-gas lines [20] and around the shaft annulus [9]. This was remedied by heating the lines and tank with heaters.

During operation of the MSRE fuel pump, transfer of salt from the pump tank to the overflow tank occurred, although the indicated salt level was 2–4 inches below the entrance of the overflow line [16]. The possible causes, likely the swelled height of the salt in the pump tank from the xenon removal salt spray system, and transfer rate dependencies are discussed in Engel et al. [16]. With respect to operation, the surge tank would occasionally need to be pressurized to return salt to the pump tank.

During operation, the salt in the primary loop had a void fraction (due to entrainment of gas in the pump tank) of <1%. The causes of gas entrainment [16] and of the gas entrainment impacts [21, 20] have been reported in detail.

Despite these occurrences, “*the operation of the salt pumps was deemed satisfactory by the MSRE Operations Group*” [9].

2.1.10 Development Path Summary

The overall progression of pump development summarized in Grindell et al. [11] is evident in separate technical reports, such as those for the MSRE pumps [9, 22].

High-temperature pumps and fluoride salt pumps, in particular, presented a number of challenges to the technology available at the time. A range of research and development activities were devoted to specific issues and specific components. The development work on these critical issues, such as the seals, was performed in parallel. Additional effort was focused on engineering solutions to liquid level control, radiation shielding, accommodating thermal expansion, and so on. The technology and lessons learned for small pumps, in both technology development and pump operation, was applied to the development of progressively larger pumps.

The ANP and MSR programs used hierarchal pump testing requirements based on the pumps’ intended purposes and experience base [11]. Pumps to be used in hot flow loops would be first subjected to cold shakedown tests. These tests determined whether the bearings, shaft and other seals, thermocouples, and seal-leakage removal system functioned satisfactorily. The performance was compared against design requirements such as the allowed shaft-seal leakage rate. The drive motor power requirements and thermocouple readings were reviewed for abnormal behavior. The LFB pumps, with considerable experience, were eventually put into service without cold testing. Pumps to be used in reactors included both cold and hot shake down testing.

Cold shakedown testing was performed on benchtop-type setup stands or in a water loop. Examples of testing, as performed for the MSRE pumps, include determining the shaft critical speed through vibration testing, measurement of the deflection of the shaft for given loads, and verifying the performance of the

seals and bearings over a range of pump operating conditions [9]. The cold testing would occur over a week or longer.

Hot tests using fluoride salts were performed in purpose-built loops separate from the reactor and were intended to find issues not apparent during cold testing. For example, the loop for testing the MSRE pumps included a cooled section, a place to insert orifices to vary the flow resistance, pressure transducers to measure the discharge pressure and the pressure drop across a venturi (for flow rate), and additional support equipment (e.g., loop heaters, thermocouples, drain tank) [9]. The hot tests included verifying the hydraulic performance recorded during water testing, testing the performance of the shaft purge gas to limit the back diffusion of radioactive gases up the shaft toward the seal, and evaluating bubble entrainment. Not performed for the MSRE pumps was cavitation inception testing, since the conditions were unlikely (the pump tank would need to be evacuated).

Ultimately, a large range of pumps were developed, tested, and put into service (Section 2.1.2).

2.2 ORNL LSTL PUMP

For the LSTL at ORNL, a centrifugal sump-type pump with an overhung impeller is used. This design eliminates the need for salt-wetted seals and salt-lubricated bearings. The pump was designed to be capable of supplying 0.125 MPa head (18 psid) at 4.5 kg/s (3.57×10^4 lbm/h) flow rate. The majority of the pump components—including the volute and the shaft—are made of the same material, Inconel-600 alloy, which provides excellent corrosion resistance under the operating conditions. The pump volute and impeller were designed by Wenesco Inc. (see Figure 2). The “volute” is actually of the concentric bowl or circular casing type and not a traditional volute. A view of the completed setup is provided in Figure 3 and Figure 4. The original design requirements for the pump were

1. Fluid: FLiNaK liquid salt at 700°C (approx.. 2019 kg/m³)
2. Flow rate: 4.5 kg/s (35 gpm @ 700oC)
3. Pump head: 20 ft of salt (17.5psi)
4. Pump construction material: Inconel 600



Figure 2. Picture of LSTL pump impeller and volute.

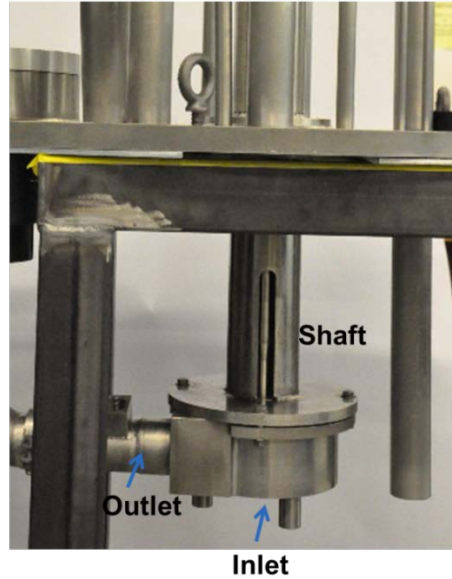


Figure 3. Picture of LSTL assembled volute.

The pump is driven through a 1,410 mm (55.5 in.) long, precision-ground drive shaft that is 50 mm (2 in.) in diameter. A John Crane–type 2800 rotating shaft seal isolates the pump sump tank’s argon cover gas from the atmosphere. The pump shaft bearing housing uses two SKF 3210-2RS bearings that are located 318 mm (12.5 in.) apart. These overhang the pump impeller by 902 mm (35.5 in.) from the centerline of the lower bearing to the top of the impeller. The pump shaft is connected to a 10 HP, 3600 RPM Brook Crompton motor through a Lovejoy flexible drive shaft (FVSLFS 1.5E). The flexible drive shaft is designed to accommodate 5 mm (0.2 in.) of axial movement and 4 mm (0.15 in.) of radial misalignment to allow axial expansion of the pump drive shaft and pump sump tank. The pump motor speed is controlled using a Lenze/AC Tech ESV752N04TFF variable-frequency drive.

Six accelerometers (IMI Sensors Model 601A01, 0.27–10 kHz) are mounted to the pump. Metal mounting pads, machined to match the contours of the bearing housing and motor, were attached using epoxy. In the future, tapped holes will be added for permanent attachment. The accelerometers were then attached to the mounting pads using screw studs. The six accelerometers are mounted at three elevations. At each elevation, two accelerometers are attached 90° apart from one another. Four are mounted to the bearing housing and two are mounted to the motor, as shown in Figure 4. A high-speed data acquisition system is set up using a National Instruments PXIe-4497 dynamic signal analyzer card. Future instrumentation could include bearing load cells and shaft position indicators.



Figure 4. Picture of pump indicating accelerometer locations.

3. PROPOSED PUMP TEST PLAN

A number of cold and hot tests have been proposed for the LSTL pump. The LSTL is located in 5800-D111 at ORNL. One proposed purpose for the tests is shakedown testing of the pump before service. However, the LSTL pump was already designed, manufactured, and installed on the LSTL before this project began. The primary purposes for the tests are to provide data to validate modeling approaches and empirical data for use in future pump designs. This section discusses these tests and the means of performing them.

3.1 COLD SHAKEDOWN TESTING

3.1.1 Test Stand Design

A cold shakedown test stand was designed for performing pump testing at room temperature using water as a surrogate working fluid. The advantages of using water at room temperature include the capability to instrument the tests well (number of instruments, high accuracy, low uncertainty, and available types), ease of visualization and inspection, and ease of pump/system modifications. A similar method of shakedown testing was adopted for the pumps developed during the ARE and MSRE programs during the 1950–1970s at ORNL (see Section 2.1.10). SINAP has also developed a water test loop for development and shakedown testing of its pumps. The cold shakedown test stand is illustrated in Figure 5. The system includes a pump, tank, piping, structural frame, and instrumentation.

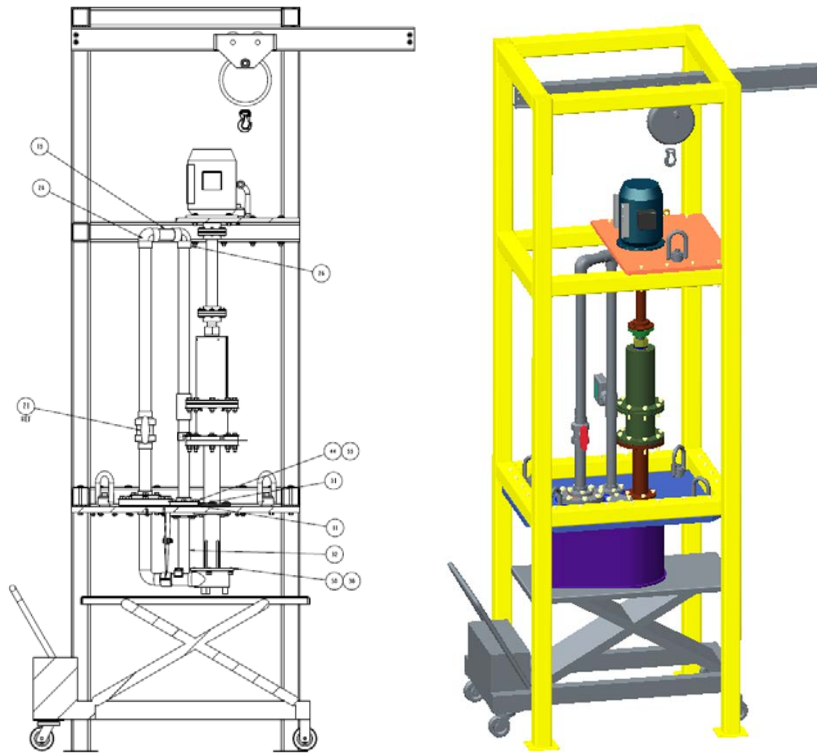


Figure 5. Pump cold shakedown test stand.

The cold shakedown test pump is directly based on the LSTL MK1 pump. However, it includes additional instrumentation and is constructed of stainless steel. The properties of stainless steel were judged to be sufficiently representative of Inconel 600 (the material of the existing pump) for the room-temperature testing. The decision to use stainless steel instead of Inconel 600 was based on available resources.

Additional flanges have been incorporated to facilitate part replacement and modification in the future. The piping includes a valve to vary the hydraulic resistance.

The tank has the same internal dimensions as the LSTL sump tank; however, it is constructed of clear acrylic to enable visualization. A table jack is used to raise and lower the tank to enable easy access to the volute and other lower structures. To facilitate unobstructed and easy removal of the tank, the metal tank lid is attached to the structural frame. The lid transfers the bearing housing and shaft load onto the structural frame instead of onto the tank. In the LSTL, the load is applied to the tank.

Instrumentation includes four pressure transducers equally spaced around the volute and two pressure transducers after the pump discharge. These provide data for code validation and to indicate the applied hydraulic loading onto the volute and piping. Accelerometers are attached in several locations on the bearing housing and motor including the locations on the LSTL. An electromagnetic flowmeter is located on the piping return leg and provides an accurate measurement of the pump flowrate. Future instrumentation plans include position sensors to record the dynamic shaft position, and bearing load cells to measure the applied loads.

3.1.2 Proposed Tests

Using the cold shakedown test stand, the following tests will be performed. The uses of the test data are briefly discussed. Ultimately, the tests provide data for model validation, inform operation of the LSTL, and provide a basis for pump design guidance.

Shaft critical speed

During dry and static conditions, an impulse hammer will be used to excite the shaft, and the vibration spectrum will be recorded. These data will be used for vibration modeling validation and to inform operation speeds (i.e., which speeds to avoid).

Shaft deflection vs. lateral load

The deflection of the shaft as a function of load will be determined under dry and static conditions. A lateral load will be placed on the impeller via a jack, ratchet, or other means, and measured. The lateral displacement of the impeller will then be measured. These data will be used for possible future structural modeling validation and to inform future gap spacing and tolerances around the impeller and shaft.

Loss of prime

The liquid level at which the pump loses prime will be determined as a function of pump speed. For a specific pump speed, the water level will be varied, with respect to the volute, until the pump loses prime. Loss of prime will be determined through visual or acoustic evidence and supported by motor power and accelerometer data. These data will inform the minimum required liquid level in the LSTL sump tank. Future uses could include the validation of CFD predictions of the sump hydraulics.

Bubble ingestion/entrainment

The entrainment of bubbles from the tank liquid free surface as a function of liquid height and pump speed will be investigated. Bubble ingestion/entrainment into the flow will be investigated through visual observation or through acoustic evidence. These data will provide information regarding the minimum required liquid level in the LSTL sump tank and indicate the presence or absence of bubbles that could impact heat transfer tests.

Hydraulic performance

The hydraulic performance of the pump will be determined. The pump flow rate and required motor power will be determined over a range of pump heads and speeds. The flow rate will be measured via magnetic flowmeter; the motor power and speed will be determined by the variable-speed drive; and the pump head will be measured via pressure transducers. The pump head will be varied by adjusting a valve on the discharge piping.

Previous work for the MSRE showed water pump head curves are directly relatable to curves developed using salt. These data will provide accurate pump curves for comparison with curves developed using the LSTL. Deviations could provide insight into LSTL flowmeter accuracy, gap, tolerances, and temperature effects.

Fountain flow

The flow through the annulus, formed by the gap between the shaft and volute, will be investigated. This parasitic flow will be estimated, as a function of pump speed and flow rate, by a weir temporarily placed around this opening. These data will aid understanding of the likelihood of bubble entrainment into the sump tank and pump and could be used in future pump and tank design guidance.

Transient characteristics (not to be performed)

The pump spin-up and coast-down time could be investigated. A range of ramp rates for the motor speed could be applied using the variable-speed drive, and motor power requirements and pump vibrations could be recorded. However, because of the small size of the pump, and the actual use of the pump, the transient spin-up and coast-down characteristics are of limited importance.

Seal and bearing endurance testing (not to be performed)

Seal and bearing endurance tests will not be performed because of the limited schedule and scope of the project. Ideally, if the tests were performed, three of the same pumps would be operated in parallel. Occasionally one pump would be disassembled and inspected for wear or other issues. The pumps would be operated for extended periods and failures noted. Such data are needed for critical service pumps (i.e., pumps for reactors or other safety significant systems); however, they are not required for the LSTL pump.

3.2 HOT TESTING

3.2.1 Loop Modification Design

To perform dedicated pump testing with the LSTL, a draft design for loop modifications has been developed. The modifications include replacing the heated silicon carbide pebble bed test section with a section of metal piping and a valve. The metal piping will connect from the pump discharge piping to the existing rotating flange below the surge tank. An additional flange, based on the existing rotating flange, is included near the sump tank lid. Like the other loop piping, the new piping will be trace heated and insulated. A valve will be used to vary the hydraulic resistance to develop pump head curves. Figure 6 illustrates the planned loop modifications.

As the valve for the loop, bellows seal, ceramic lined/ball, and cryogenic types of valves were considered. The valve selection is not straightforward, primarily because of availability issues (cost and manufacturing timeframe) for valves constructed of salt-compatible materials. A 1.5 in., 300 lb Hastelloy

C-276 globe valve with an extended bonnet was selected. The performance of the stem packing and of the valve in general will be evaluated through the course of the testing.

The new piping, seamless Inconel 600 1.5 in. sch 40, will include flats to facilitate installing an ultrasonic flowmeter. This will provide additional space and an alternate pipe size (1.5 in. vs. 1.0 in.) for testing flowmeter performance.

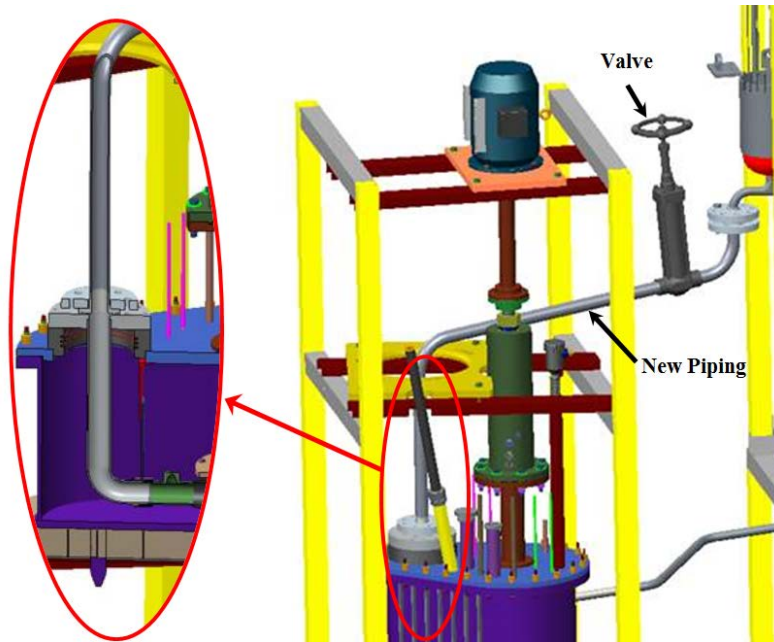


Figure 6. Illustration of LSTL modification for pump testing.

3.2.2 Proposed Testing

Hydraulic performance verification

The pump head vs. flow vs. speed curves will be determined. At a set valve position, the pump speed will be varied. The discharge pressure, flow rate, salt temperature, and motor power will be recorded. These curves will be developed for 550–700°C salt temperatures. These data will later be used in validating CFD model predictions (see Section 4.1).

During these tests, the temperatures of the top of the tank, the bearing housing, the bearings, and the area near the seal will be recorded. These data are useful for understanding the thermal loads on the bearings and seal. Future pump modifications and designs could incorporate features to reduce and/or control temperatures at these locations. The data could also be used in future validation of thermal modeling of the pump or as input to structural modeling of the pump.

During these tests, vibration data from the accelerometers will be recorded. These data will later be used to validate model predictions for the pump (see Section 4.2). In addition, by comparing the data over time, the data could indicate issues (bearing failure, rubbing) that arise with the pump.

Endurance testing (not to be performed)

Actual endurance testing will not be performed because of the long run time it would require. Data (such as vibration spectra and amplitude and motor power requirements) from initial operation will be

compared periodically with data over the course of LSTL operation. The data will be compared to identify any issues that arise over the life of the pump.

4. PERFORMANCE CHARACTERISTICS OF THE LSTL PUMP MK1

As of this writing, the LSTL pump has not operated in salt and the cold shakedown test stand has not been fabricated. Thus, there are limited data available on the performance of the LSTL pump. The hydraulic and vibration characteristics of the pump were selected for investigation through modeling. Models and predictions of the hydraulic (Section 4.1) and vibration (Section 4.2) performance of the pump have been developed. Later, data from pump testing will be used to validate the modeling approaches. The thermal and structural characteristics of the pump may also be evaluated in future work. Finally, after the test data and model validation results are obtained, guidelines for future salt pump design will be formalized.

4.1 PREDICTED HYDRAULIC PERFORMANCE

A CFD model was developed and used to predict the hydraulic performance of the LSTL pump. The intent was to use the LSTL pump to provide data to validate the model. Later, this modeling approach will be used in the design of a new pump impeller and volute. Currently salt test data are not available to perform the validation. The following subsections summarize the CFD modeling and results for the LSTL pump.

4.1.1 Computational Fluid Dynamics Model

A CFD model was developed in the COMSOL Multiphysics 5.2 [23] software to assess the steady state performance of ORNL MSL pump operation. The CFD model geometry was prepared using a CAD model of the pump (Figure 7) and hence was accurate according to the drawing specifications. Both the inlet and outlet of the CFD model were geometrically extended to provide a numerically stable set of boundary conditions. As shown in Figure 8, the pressure at the inlet, the pressure around the shaft-casing peripheral gap, the flow rate at the discharge outlet, and the rotational speed of the impeller were specified as the boundary conditions.

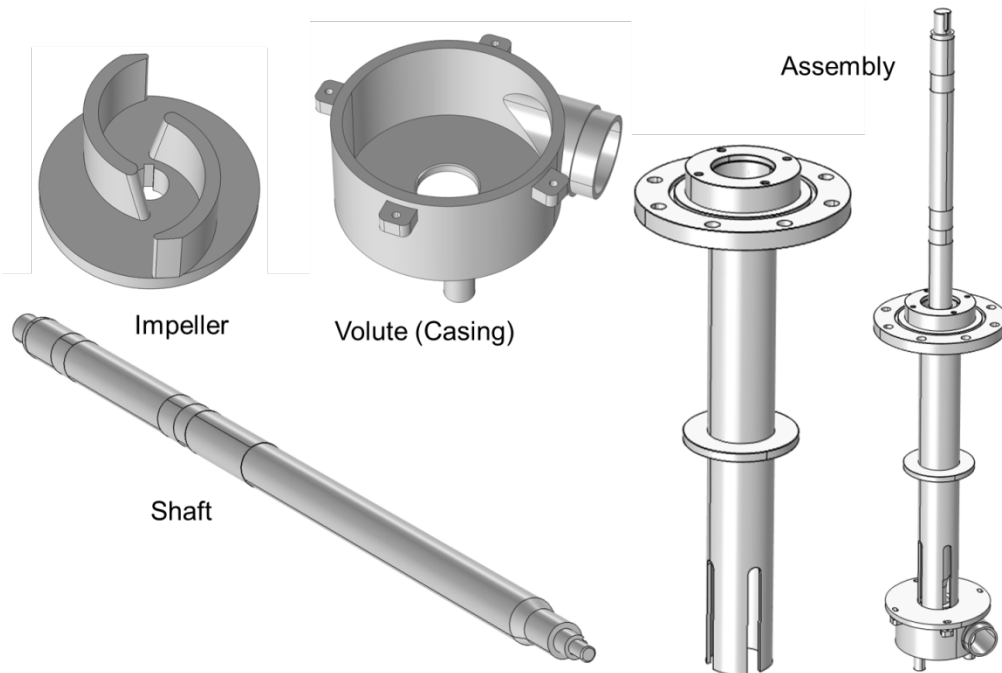


Figure 7. A detailed CAD model for the ORNL molten salt pump assembly.

The rotating machinery and turbulent flow interfaces within the CFD module of COMSOL Multiphysics were used to model the pump behavior. COMSOL provides two different solution schemes for pump models: (1) time-dependent approach and (2) pseudo-steady frozen rotor approach.

Time-dependent approach

In the time-dependent rotating machinery interface, the governing Navier-Stokes equations that describe the conservation of mass and momentum are formulated in a rotating coordinate system and written as [23] the following.

Continuity equation (in a rotating coordinate system):

$$\frac{\partial \rho}{\partial t} + \nabla \cdot (\rho \mathbf{v}) = 0 \quad (1)$$

Momentum equation (in a rotating coordinate system):

$$\rho \frac{\partial \mathbf{v}}{\partial t} + \rho (\mathbf{v} \cdot \nabla) \mathbf{v} + 2\rho \boldsymbol{\Omega} \times \mathbf{v} = \nabla \cdot [-p\mathbf{I} + \boldsymbol{\tau}] + \mathbf{F} - \rho \left(\frac{\partial \boldsymbol{\Omega}}{\partial t} \times \mathbf{r} + \boldsymbol{\Omega} \times (\boldsymbol{\Omega} \times \mathbf{r}) \right) \quad (2)$$

where p is pressure, ρ is density, t is time, \mathbf{v} is the velocity vector in the rotating coordinate system, $\mathbf{r} = \mathbf{x}(\boldsymbol{\Omega}, t)$ is the position vector, $\boldsymbol{\Omega}$ is the angular velocity vector, $\boldsymbol{\tau}$ is the viscous stress tensor, \mathbf{I} is the identity matrix, ∇ is a vector differential operator, and \mathbf{F} is the volume force vector.

The relation between \mathbf{v} and the velocity vector in the stationary coordinate system \mathbf{u} is

$$\mathbf{u} = \mathbf{v} + \frac{\partial \mathbf{r}}{\partial t} \quad (3)$$

which can be used to reformulate Eqs. (1) and (2) in terms of a nonrotating (stationary) coordinate system to yield the following equations.

Continuity equation (transformed to a stationary coordinate system):

$$\frac{\partial \rho}{\partial T} - \frac{\partial \mathbf{x}}{\partial T} \cdot \nabla \rho + \nabla \cdot (\rho \mathbf{u}) = 0 \quad (4)$$

Momentum equation (transformed to a stationary coordinate system):

$$\rho \left(\frac{\partial \mathbf{u}}{\partial T} - \frac{\partial \mathbf{x}}{\partial T} \cdot \nabla \mathbf{u} \right) + \rho (\mathbf{u} \cdot \nabla) \mathbf{u} = \nabla \cdot [-p\mathbf{I} + \boldsymbol{\tau}] + \mathbf{F} \quad (5)$$

where $\frac{\partial \rho}{\partial T}$ and $\frac{\partial \mathbf{u}}{\partial T}$ are the mesh time derivative of the density and velocity, respectively.

In fixed nonrotating domains, the ordinary Navier-Stokes equations are solved, with the rotating and fixed parts coupled together through an identity pair to enforce a continuity boundary condition.

In COMSOL, both Eqs. (4) and (5) are solved using a time-dependent solver.

Frozen rotor approach

For pseudo-steady simulations, a frozen rotor approach was used which assumes the rotating domain (a cylindrical domain that encloses the impeller) to be in a fixed (or frozen) state while appropriately transforming the governing equations and boundary conditions to model the rotational behavior. In nonrotating domains, however, the ordinary stationary Navier-Stokes equations were solved.

In general, for most rotating machinery problems, there are no steady state solutions; and only a pseudo-steady solution can be achieved that varies periodically around an average value. The pseudo-steady solution depends on the position in which the impeller is frozen. Therefore, it is recommended that time-dependent simulations be performed to achieve a more accurate stationary state. However, the pseudo-steady solution obtained from the frozen rotor approach can be used as an initial condition to the time-dependent model to accelerate numerical convergence.

In the frozen rotor approach, the flow in the rotating domain is assumed to be fully developed, or time invariant. This assumption reduces the governing equations in (1) and (2) to the following [23]:

Continuity equation (frozen rotor):

$$\nabla \cdot (\rho \mathbf{v}) = 0 \quad (6)$$

Momentum equation (frozen rotor):

$$\rho(\mathbf{v} \cdot \nabla)\mathbf{v} + 2\rho\boldsymbol{\Omega} \times \mathbf{v} = \nabla \cdot [-p\mathbf{I} + \boldsymbol{\tau}] + \mathbf{F} - \rho\boldsymbol{\Omega} \times (\boldsymbol{\Omega} \times \mathbf{r}) \quad (7)$$

In COMSOL, both Eqs. (6) and (7) are transformed to a stationary coordinate system and solved using a steady state solver.

4.1.2 Boundary Conditions for the CFD Model

The boundary conditions for the pump CFD model (Figure 8) are provided in Table 2.

Table 2. CFD boundary conditions

Boundary condition	Value	Remarks
Pressure at suction inlet	0 atm	Relative pressure
Velocity at discharge outlet	1 m/s, 3 m/s, 5 m/s	For varying discharge flow rates
Pressure at shaft periphery	$P_{\text{inlet}} - \rho gH$	Subtract static gravitational head
Flow continuity	Identity pair between the rotating and stationary domains	Continuity at the rotating and non-rotating assembly interface
Rotational speed	1750 rpm	Revolutions per minute
Walls	No-slip with wall functions	k-ε turbulence model

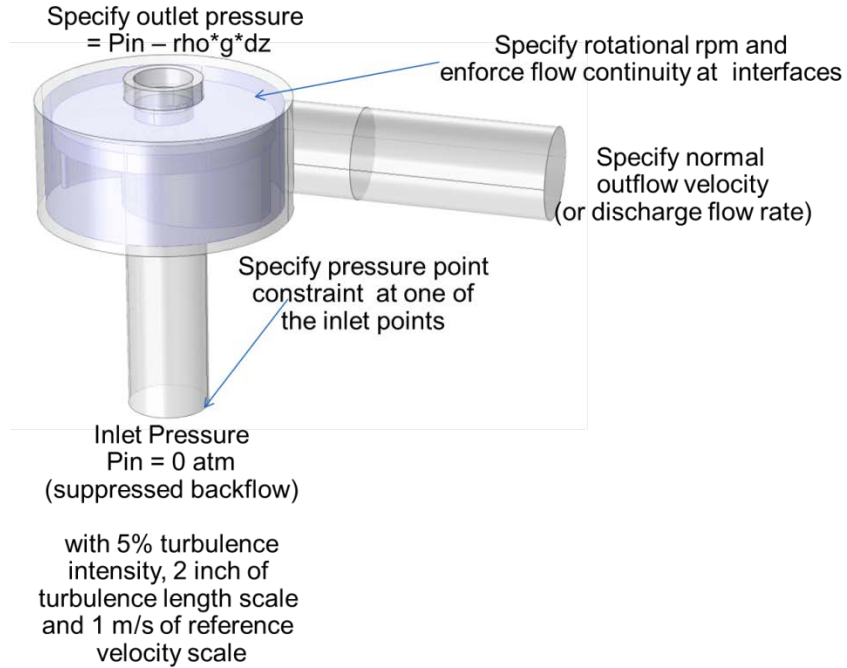


Figure 8. Description for the CFD model boundary conditions.

4.1.3 Numerical Mesh for the CFD Model

A free tetrahedral, finite element, linear-basis mesh was generated for the CFD model geometry, as shown in Figure 9. The element size parameters used to construct the mesh are provided in Table 3.

Table 3. COMSOL CFD mesh setup

Mesh parameters	Value
Maximum element size	0.05 m
Minimum element size	0.01 m
Maximum element growth rate	1.15
Curvature factor	0.025
Resolution of narrow regions	0.5
Number of boundary layers	6
Boundary layer stretching factor	1.2

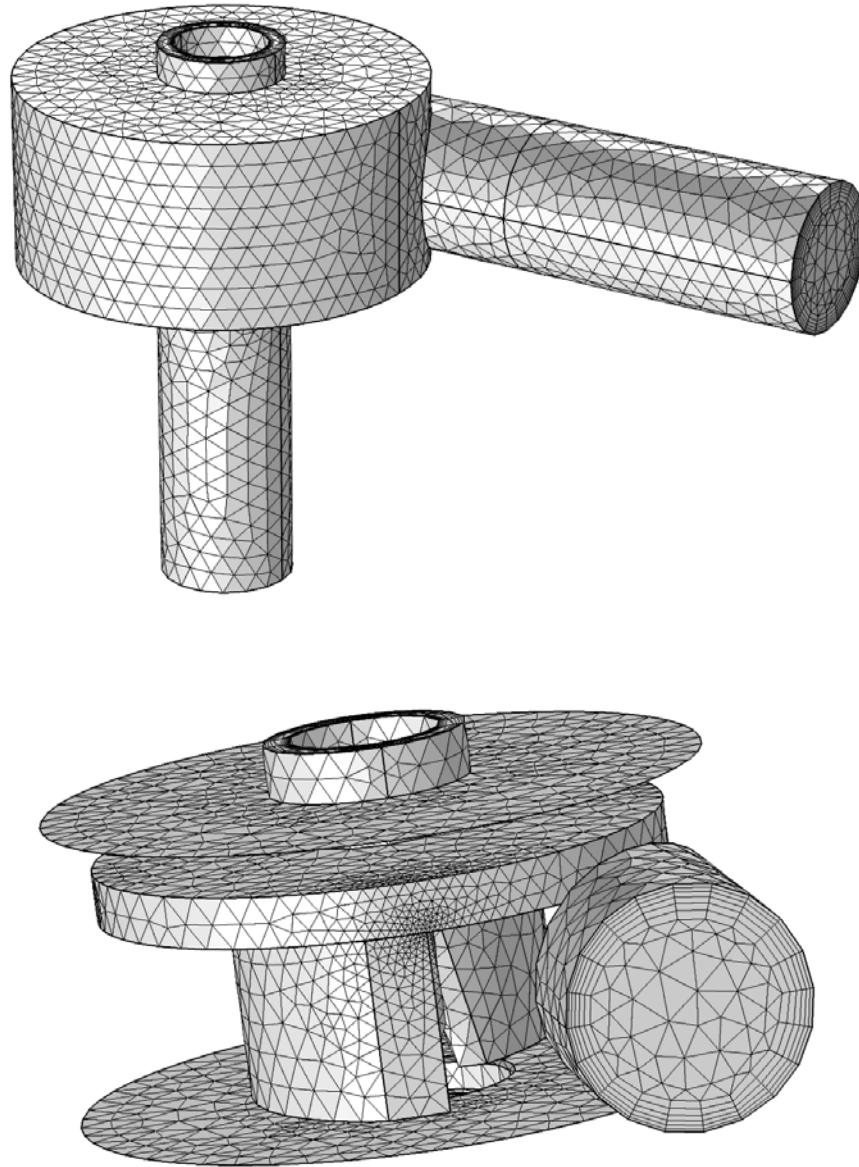


Figure 9. Free tetrahedral finite element mesh with boundary layers for the pump CFD model. This mesh results in a wall lift off (in viscous units) y^+ value of 11.1, in compliance with the specific k-e model implemented in COMSOL.

4.1.4 Material Properties for the Molten Salt

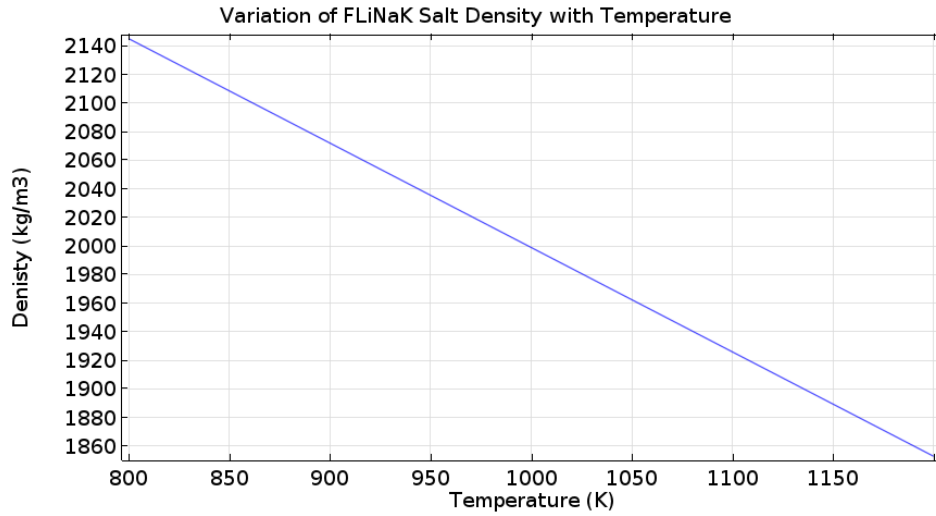
For the FLiNaK molten salt, the following equations provide the variation of density and dynamic viscosity with temperature [24] and are plotted in Figure 10:

$$\text{Density: (kg/m}^3\text{)} \quad \rho = -0.73 T + 2729 \quad (8)$$

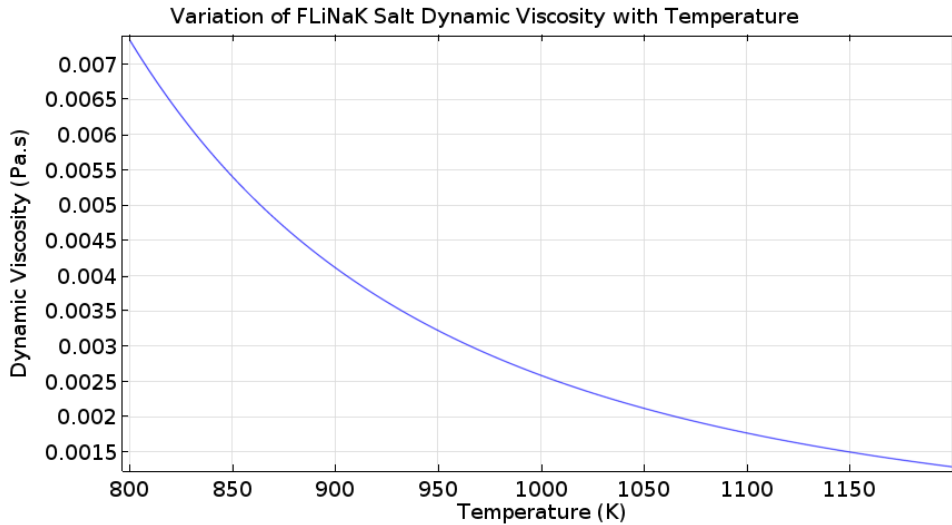
$$\text{Dynamic viscosity: (Pa}\cdot\text{s)} \quad \mu = 4 \times 10^{-5} e^{4170/T} , \quad (9)$$

where temperature T is in K.

A temperature of 675°C (948 K) was chosen for the molten salt in the CFD simulations.



(a) Density



(b) Dynamic viscosity

Figure 10. Variation of FLiNaK salt properties with temperature.

4.1.5 Pseudo-Steady CFD Results

Steady state simulations were performed using the frozen rotor approach at 1,750 rpm for varying discharge flow rates. In the frozen rotor approach, the rotating flow is simulated by assuming a fixed, or frozen, topology of the impeller relative to its rotating frame of reference. This assumption significantly reduces the computational resources required to simulate the pseudo-steady state condition. This approach is equivalent to solving the stationary Navier-Stokes equations where centrifugal and Coriolis forces have been added to the rotating domains.

Typical flow streamlines obtained from the frozen rotor CFD simulations are shown in Figure 11. The molten salt is drawn in through the vertical inlet into the volute chamber, where it rotates according to the specified speed and is ejected through the horizontal discharge outlet.

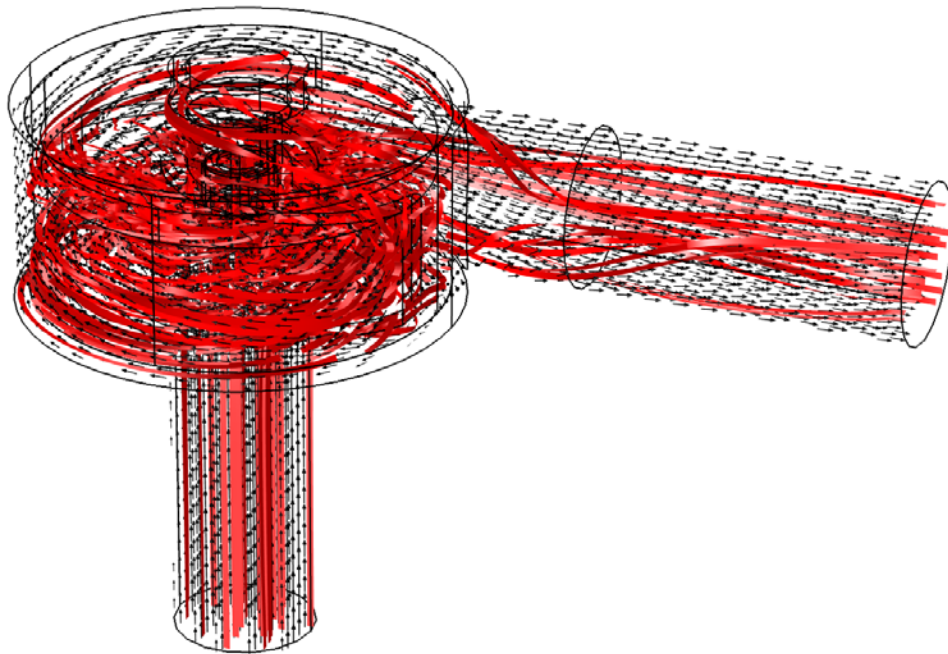
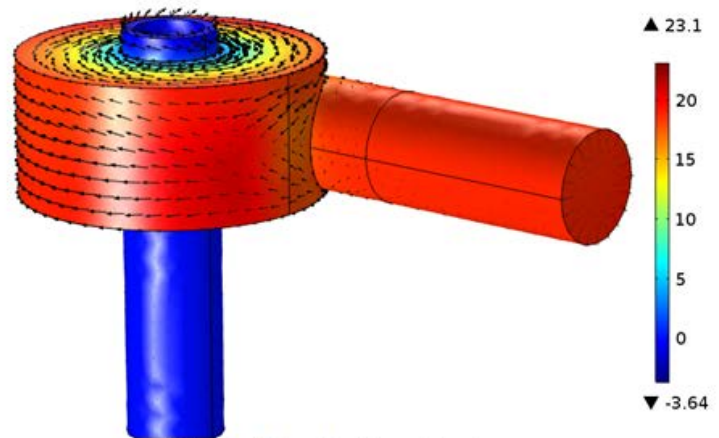
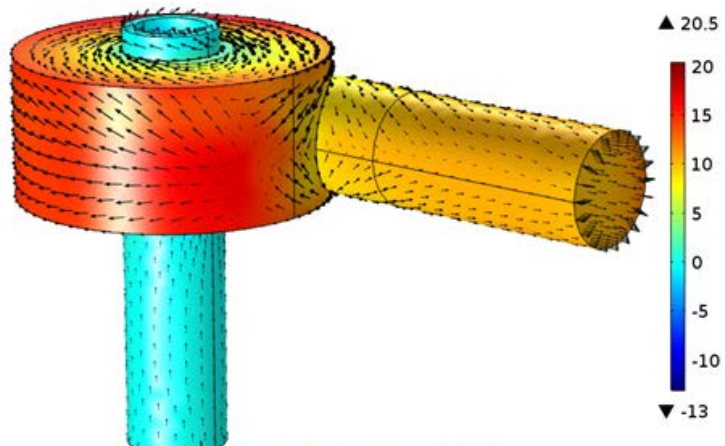


Figure 11. Typical flow streamlines as predicted by the pump CFD model.

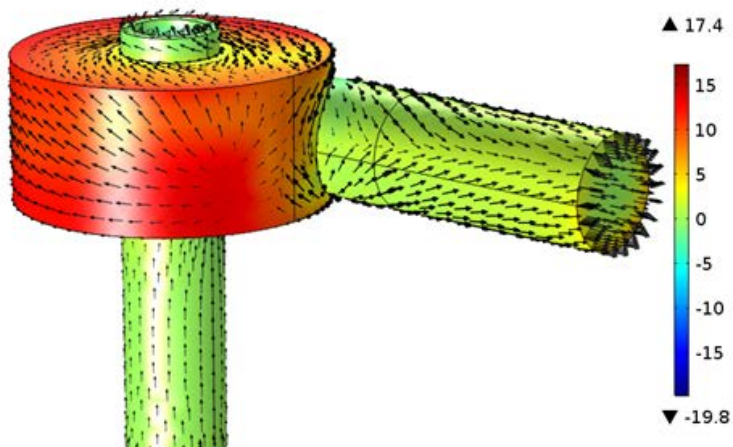
Three-dimensional (3-D) pseudo-steady pressure distribution for different discharge velocities (1 m/s, 3 m/s and 5 m/s) are shown in Figure 12 and Figure 13. As expected, a considerable pressure reduction occurs in near-blade regions (see Figure 13); it could cause cavitation (boiling) in some liquids if the local pressure should drop below its respective saturated vapor pressure. However, for the molten FLiNaK salt, cavitation does not pose a problem because of the salt's significantly low saturated vapor pressure (low volatility). FLiNaK salt, with a percentage molar composition of LiF(46.5)–NaF(11.5)–F(42), has a melting point of 454°C, a boiling point of 1,570 °C, and a very low saturated vapor pressure of 0.7 mm Hg at 900°C [24].



(a) Outlet velocity = 1 m/s

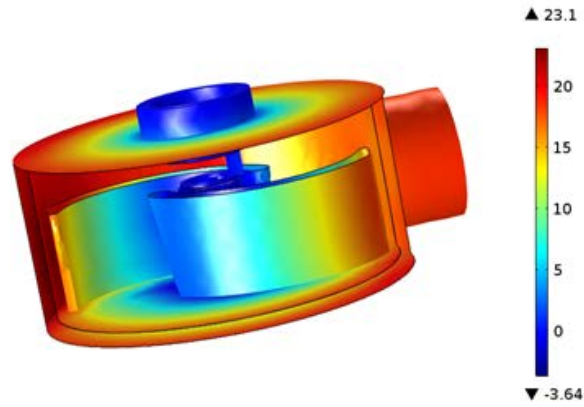


(b) Outlet velocity = 3 m/s

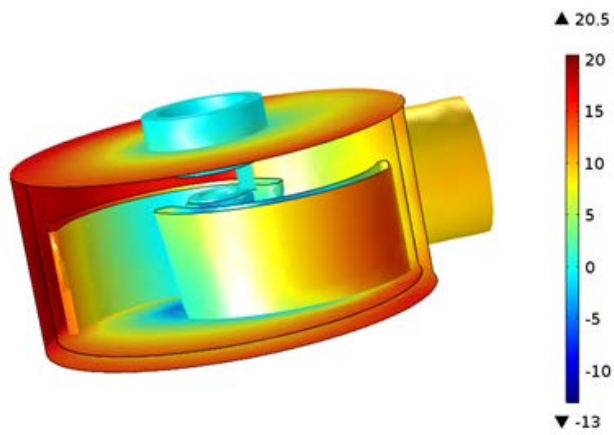


(c) Outlet velocity = 5 m/s

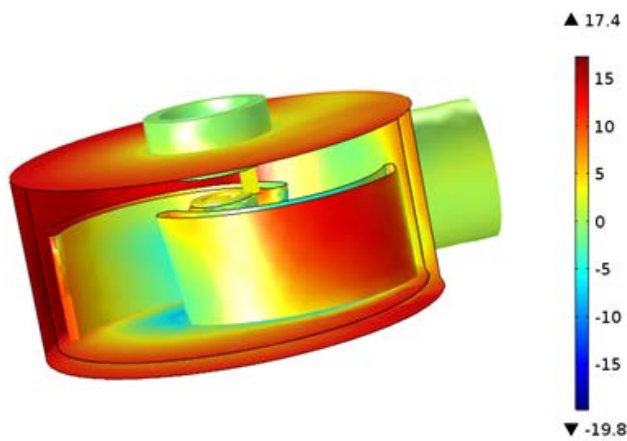
Figure 12. Pseudo-steady pressure (psi) distribution at 1,750 rpm for different outlet discharge rates.



(a) Outlet velocity = 1 m/s



(b) Outlet velocity = 3 m/s



(c) Outlet velocity = 5 m/s

Figure 13. Pseudo-steady pressure (psi) distribution at 1,750 rpm for different outlet discharge rates.

Three-dimensional CFD results were also post-processed at select vertical and horizontal cut planes through the pump (see Figure 14). The corresponding surface contour plots for pressure and velocity are provided in Figure 15 and Figure 16 for different discharge flow rates at 1,750 rpm.

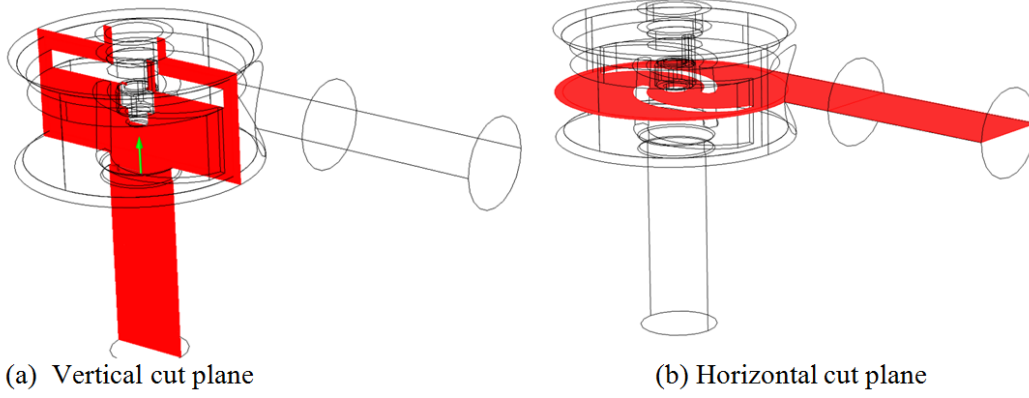
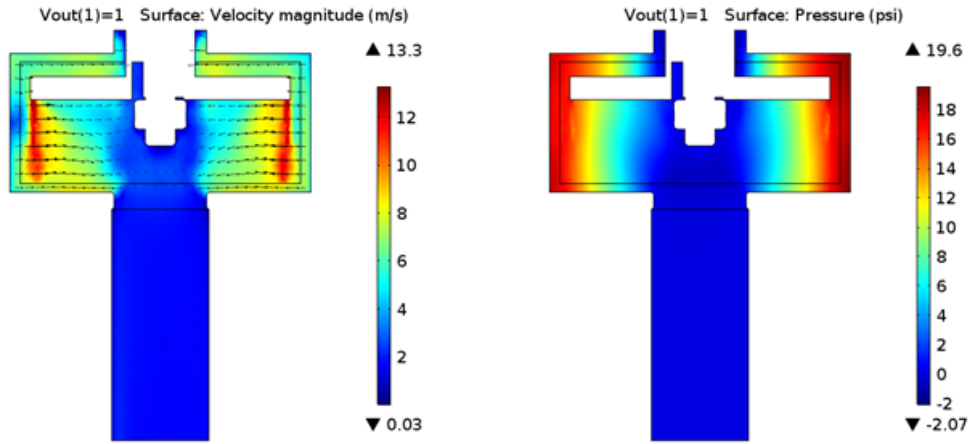
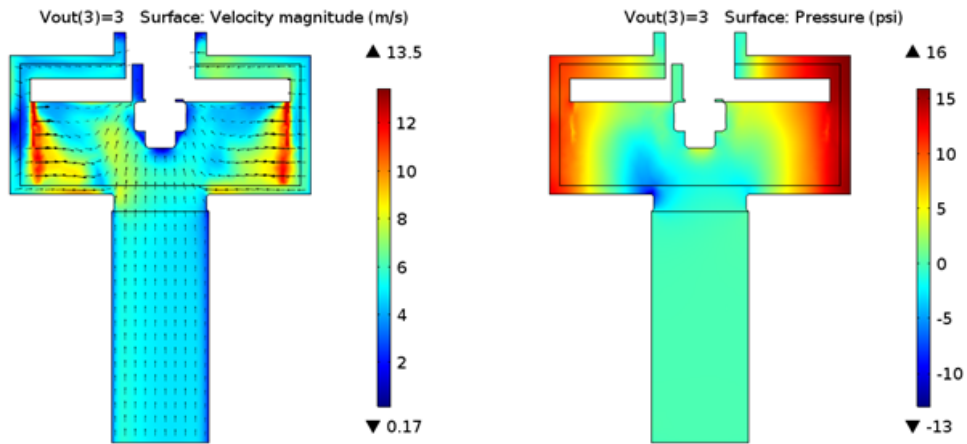


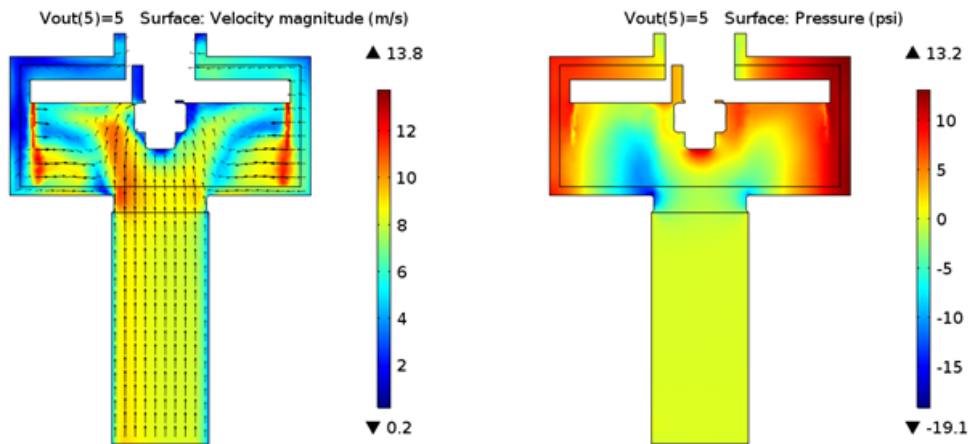
Figure 14. The locations of vertical and horizontal cut planes for visualizing CFD results.



(a) Outlet velocity = 1 m/s



(b) Outlet velocity = 3 m/s



(c) Outlet velocity = 5 m/s

Figure 15. Velocity (m/s) and pressure (psi) contours for different discharge rates, plotted on a vertical cut plane through the pump operating at 1,750 rpm.

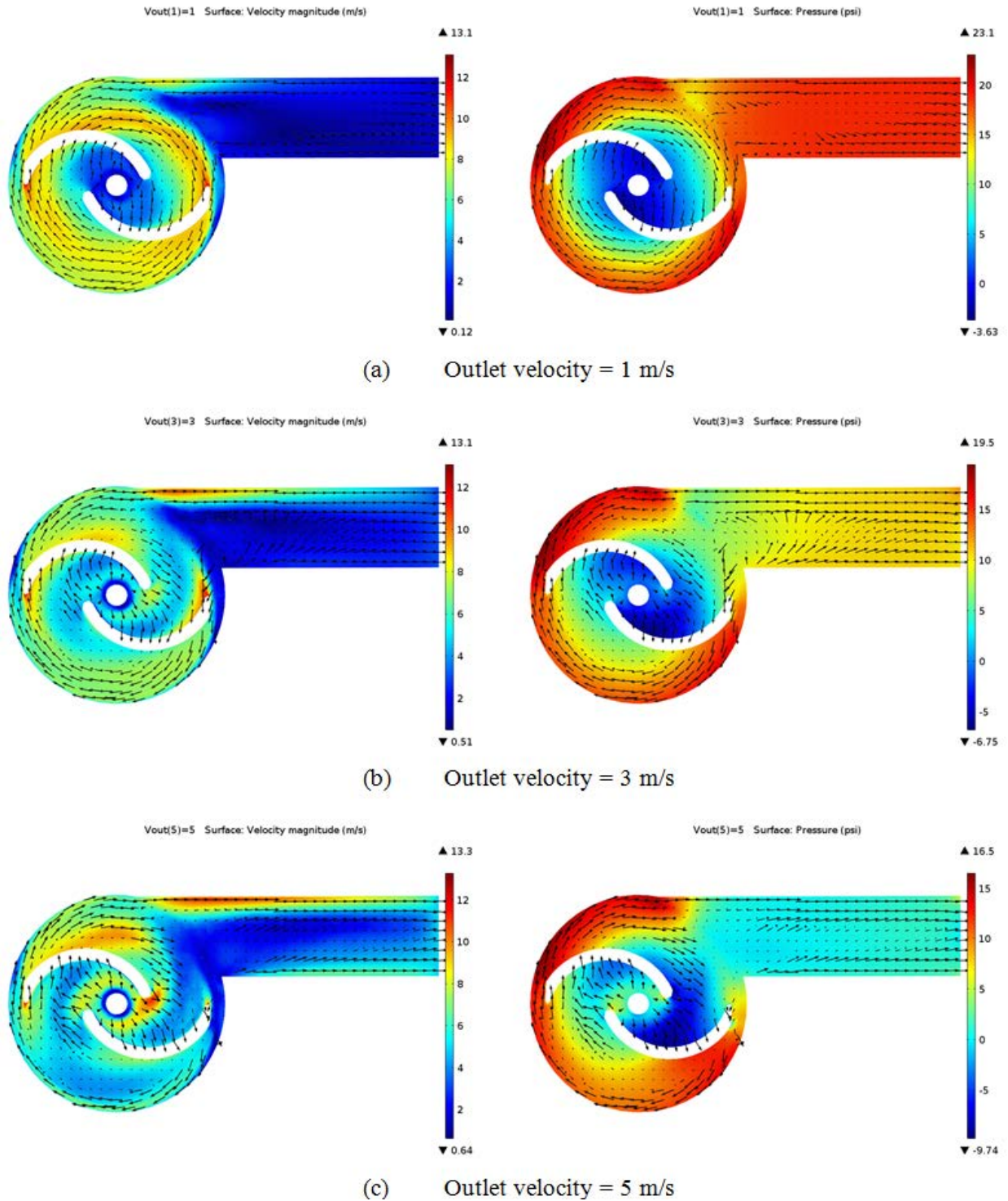


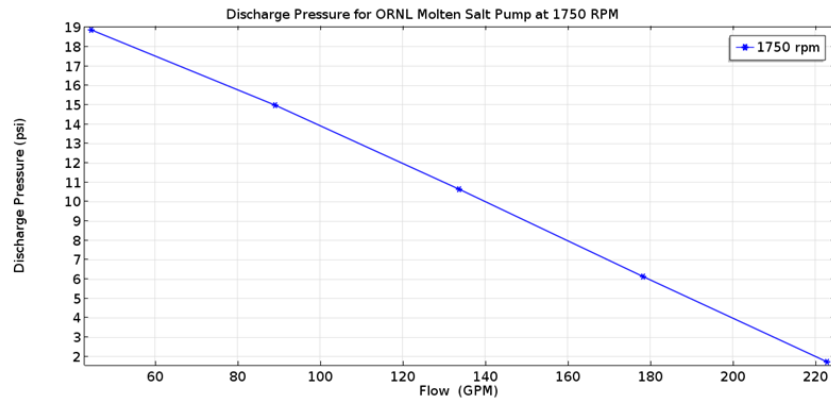
Figure 16. Velocity (m/s) and pressure (psi) contours for different discharge rates, plotted on a horizontal cut plane through the pump operating at 1,750 rpm.

The pump performance curve at 1,750 rpm for the variation of average discharge pressure as a function of the discharge flow rate is provided in Figure 17(a). By applying the Bernoulli equation between the inlet and the outlet of the pump, the total head produced by the pump can be calculated:

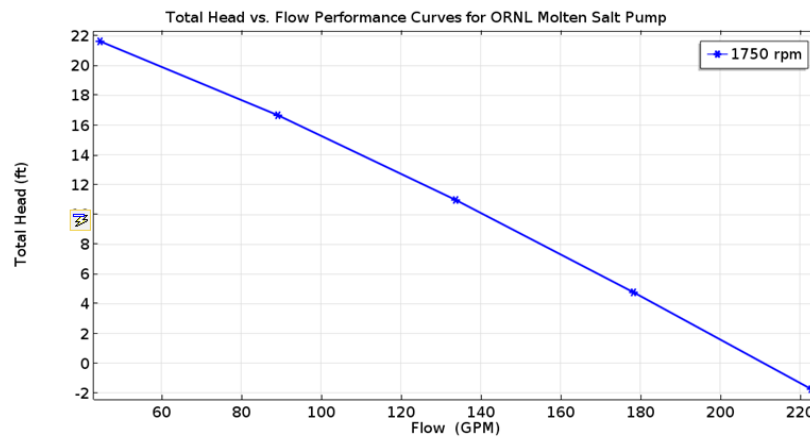
$$Total\ head\ \Delta H = \left(\frac{p}{\rho g} + \frac{V^2}{2g} + z \right)_{outlet} - \left(\frac{p}{\rho g} + \frac{V^2}{2g} + z \right)_{inlet} , \quad (10)$$

where p is the pressure, V is the velocity magnitude, z is height, and g is the gravitational constant.

The total head calculated from the CFD model at 1,750 rpm is plotted against the flow rate in Figure 17(b).



(a) Discharge pressure vs. flow



(b) Total head vs. flow

Figure 17. Pump performance as predicted by the CFD model at 1750 rpm.

4.1.6 Pump Affinity Laws

Once the pump performance is established for a given rotational speed, the pump affinity (or similarity) laws [25] can be applied to estimate its performance at other speeds. The pump affinity law states that, for incompressible flow conditions, the discharge flow capacity varies with the ratio of pump rotational speeds and the total head varies with the square of this ratio.

The affinity law can be written as follows [25]:

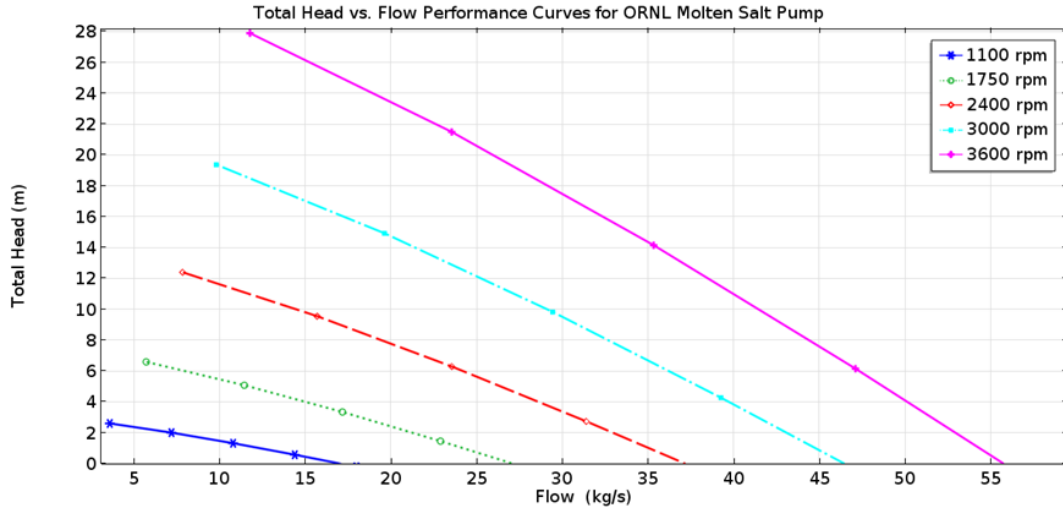
$$\begin{aligned}
 Q_2 &= Q_1 \left(\frac{rpm_2}{rpm_1} \right) \\
 \Delta H_2 &= \Delta H_1 \left(\frac{rpm_2}{rpm_1} \right)^2
 \end{aligned}
 \tag{11}$$

where Q is the volumetric flow rate, ΔH is the total head, and rpm is the rotational speed of the pump. Using Eq. (11), the pump performance results at 1,750 rpm were translated for other rotational speeds of interest and are provided in Figure 18 in both SI and US customary units. Once the pump performance is known at a given speed, the power imparted to the liquid by the rotating impeller can be calculated from Eq. (12):

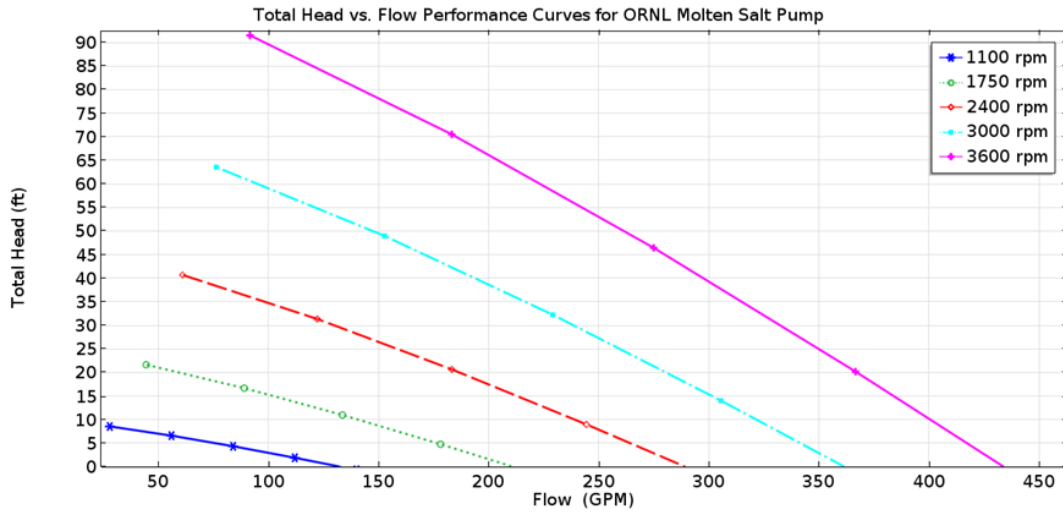
$$Power_{liquid} = \dot{m}g\Delta H ,
 \tag{12}$$

where \dot{m} is the mass flow rate.

The power imparted to the molten salt for different operating speeds is plotted against the flow rate in Figure 19. The efficiency of the pump can now be determined by dividing the liquid power by the power supplied to the ORNL pump (i.e., from a 10 hp motor) and is plotted in Figure 20 for different operating speeds.

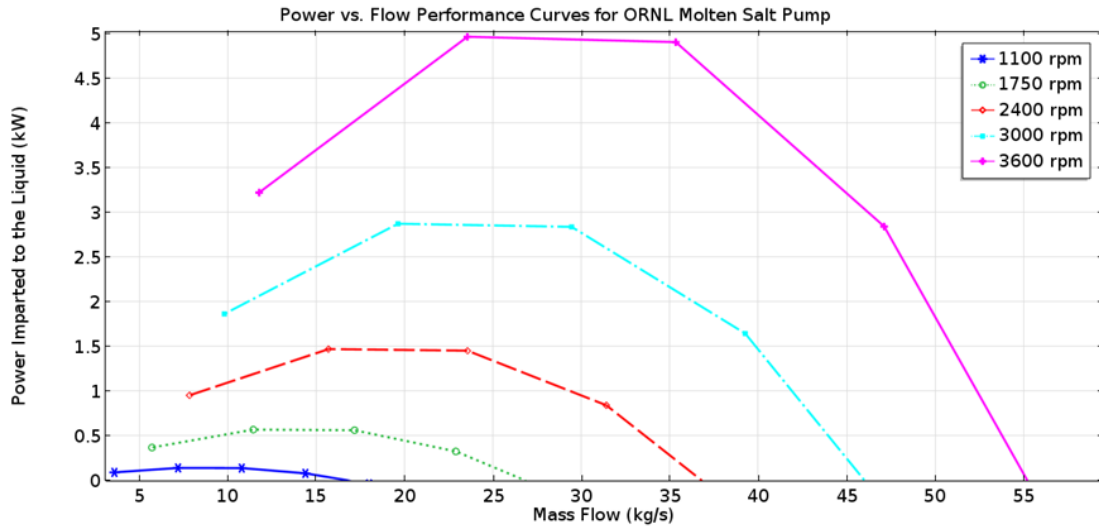


(a) SI units

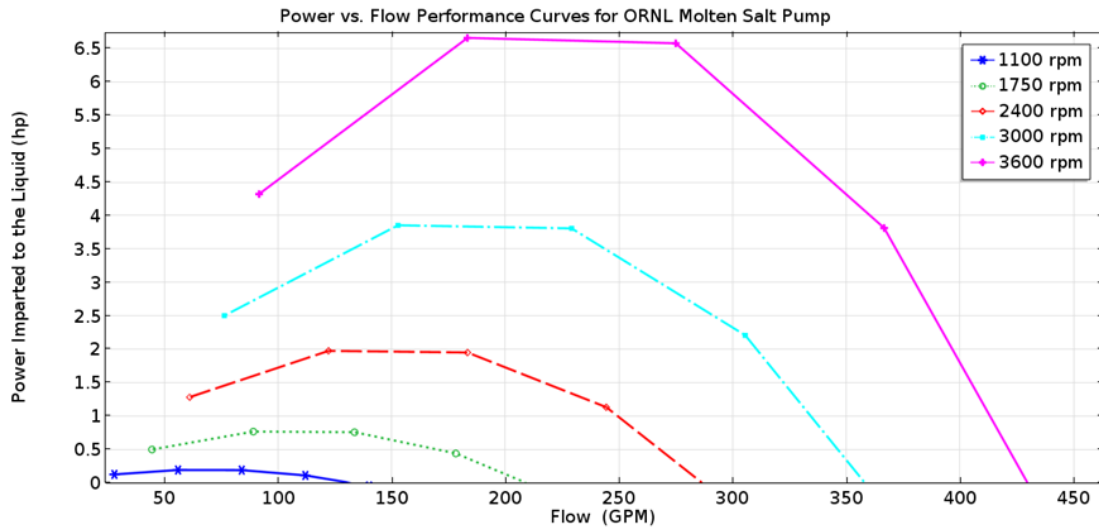


(b) US customary units

Figure 18. Head flow performance curves for the ORNL pump—as predicted by the CFD model.



(a) SI units



(a) US customary units

Figure 19. Power imparted to the liquid by the pump for different operating speeds, as predicted by the CFD model.

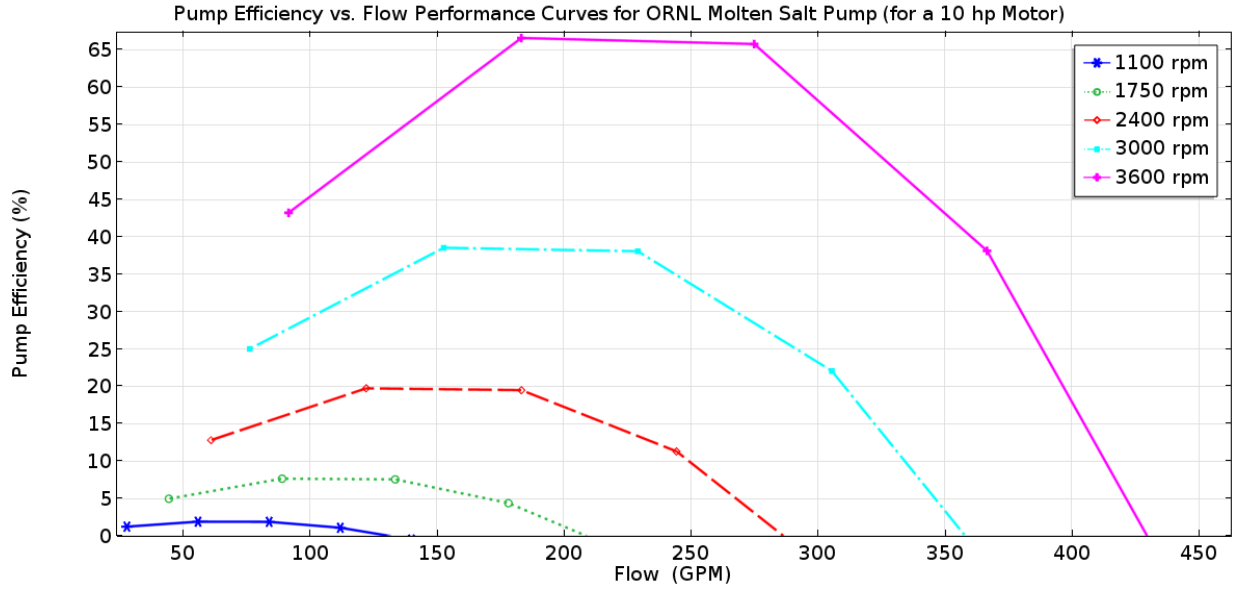


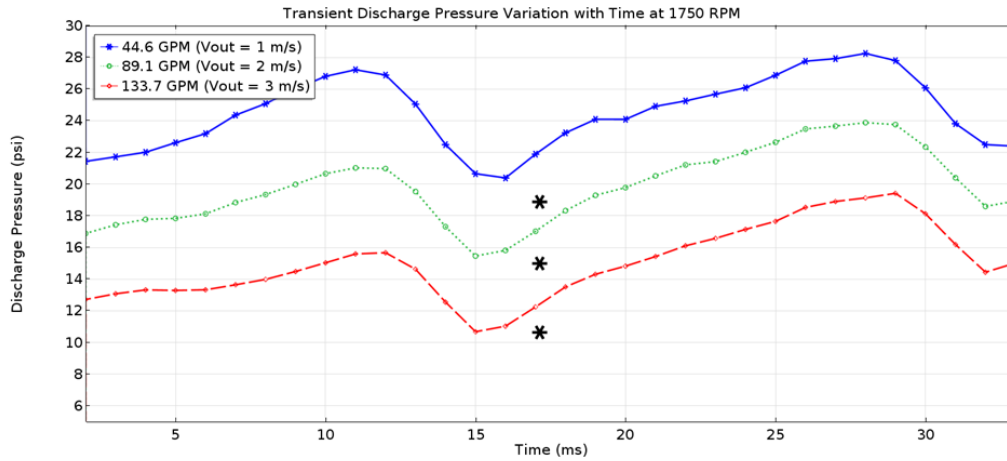
Figure 20. Pump efficiency results for different operating speeds—as predicted by the CFD model.

4.1.7 Time-dependent CFD results

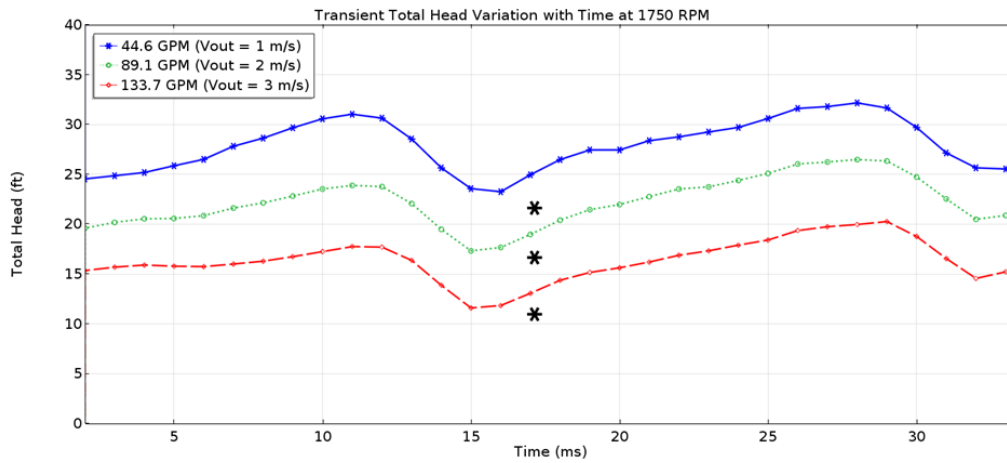
A time-dependent CFD simulation for 33 ms duration, equivalent to a full 360° revolution of the impeller, was performed for the pump speed of 1,750 rpm. The time-dependent model was initialized by the pseudo-steady solution obtained from the frozen rotor model. This model accounts for the movement of the geometrical parts (e.g., impeller and casing) relative to each other and provides a more accurate way to simulate the pump performance. In the model, the impeller is surrounded by a rotating domain, whereas the inlet, outlet and the casing walls are parts of a nonrotating domain. Both of these domains are integrated by a sliding mesh interface on which a flow continuity condition is enforced. In general, the time-dependent approach is significantly expensive compared with the frozen rotor approach for simulating the normal operation under pseudo steady state conditions.

The CFD results from the time-dependent model are provided in Figure 21, which shows the time-dependent oscillations of the discharge pressure and the total head. As depicted by the asterisks (*) in the figure, the corresponding pseudo-steady values, obtained from the frozen rotor model, lay slightly below the average of transient variations.

Temporal pressure profiles at $t = 2$ ms, 10 ms, and 30 ms are also provided in Figure 22 for a horizontal cut plane through the pump.



(a) Discharge pressure vs. time



(b) Total head vs. time

Figure 21. Time-dependent CFD model results at 1,750 rpm for the pump discharge pressure and total head for three different discharge rates. The asterisks (*) indicate their corresponding steady state values as obtained from separate frozen rotor simulations.

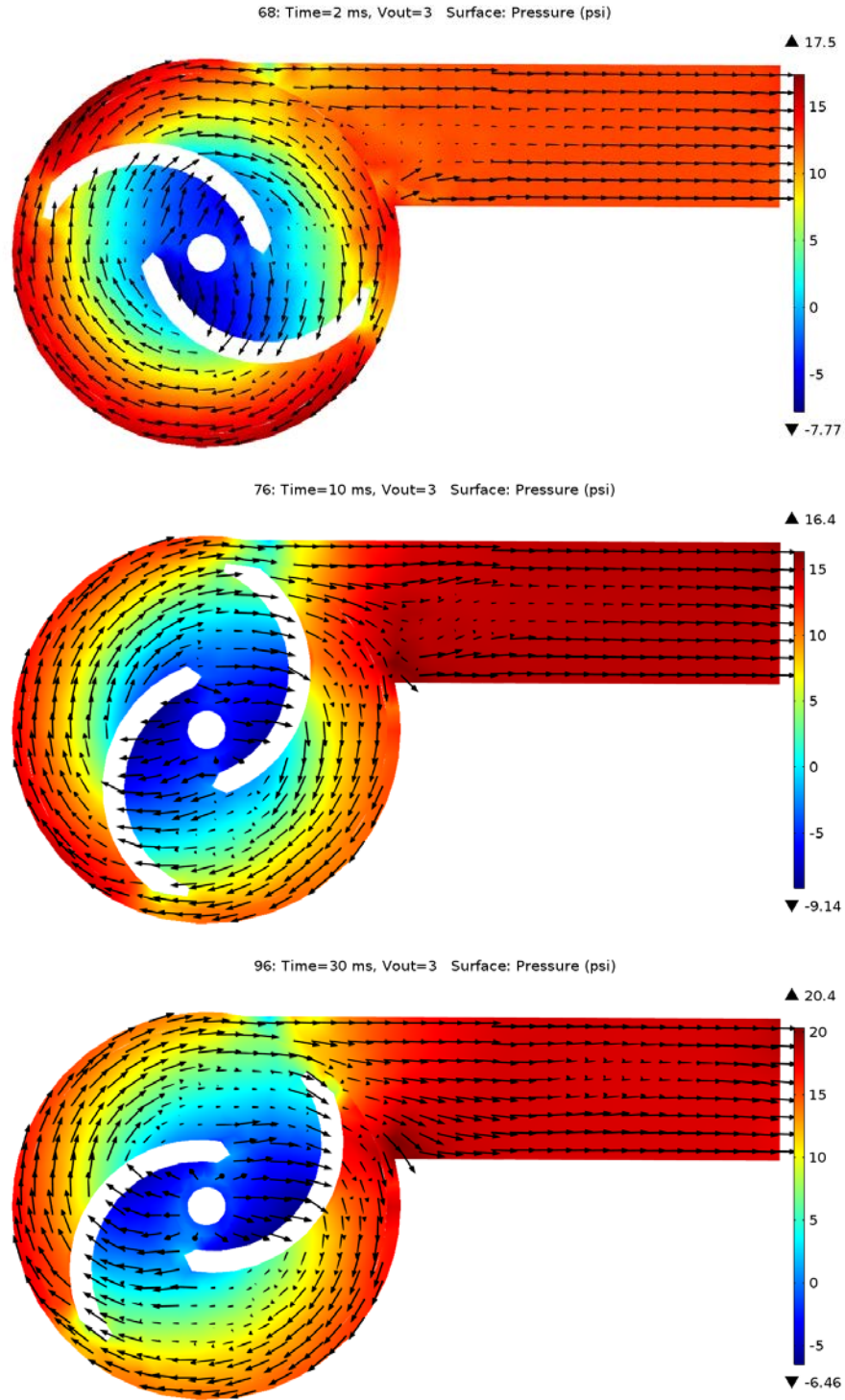


Figure 22. Time-dependent pressure (psi) variation on the horizontal cut plane at different times: (a) $t = 2$ ms, (b) $t = 10$ ms, and (c) $t = 30$ ms (pump operating speed = 1,750 rpm and discharge velocity = 3 m/s).

4.2 PREDICTED SHAFT VIBRATION CHARACTERISTICS

To prepare an accurate model of the salt pump for modal analysis and design optimization, it is beneficial to confirm that a simple beam element model produces similar results to a more complex 3-D model. The purpose of these calculations is to compare the two models and to begin to validate them against the empirical impact test data. For this purpose, the salt pump shaft was chosen as a starting point for this comparison and validation.

4.2.1 Modeling Assumptions

Boundary conditions

The centerline circumference at the location of each of the two bearings is assumed to have a fixed displacement for both models of the shaft. The fixed boundary conditions are equivalent to assuming that the bearings and their supporting column are infinitely stiff. This is a good starting point for a comparison of the two models. The fixed boundary condition will be modified during the validation of the full model to include a spring element that is equivalent to the bearing stiffness.

Load

It is assumed there is no loading of the shaft. The unloaded shaft will be adequate for the purpose of this preliminary model comparison. The shaft will eventually have compression fittings and impeller mass and will be combined with the larger model through the coupling. Rotation and fluid forces have not been considered in these models so as to replicate the impact test conditions.

4.2.2 Calculation Input

Materials and material properties

The salt pump shaft is made of Inconel 600 and the properties are shown in Table 4 [26].

Table 4. Inconel 600 mechanical properties for vibration analyses

Property	Value
Density	0.304 lb/in. ³
Young's modulus	31 × 10 ³ ksi (at 70°F)
Poisson's ratio	0.29 (at 70°F)

Geometry

The salt pump shaft is essentially a stepped shaft of varying diameter. For modeling purposes, the threading and keyways on the ends have been omitted.

Beam model

The ANSYS finite element code was used for the analysis of the salt pump shaft. The element type "Beam189" was used to model the shaft, because this element type is appropriate for moderately thick beam structures and has the option for a circular cross section. The elements have three nodes with six degrees of freedom on each node. The distance between nodes was chosen to be 0.025 m.

3-dimensional model

The 3-D model was created using ANSYS Workbench v16.2 from the imported shaft model Figures 24–26). The meshing method used was the Hex Dominant method. The default sizing was more than sufficient for modal analysis purposes.



Figure 23. Three-dimensional shaft model mesh.

Geometry
4/19/2016 11:45 AM



Figure 24. Three-dimensional geometry.

A: Modal
Fixed Support
Frequency: N/A
4/19/2016 11:44 AM

Fixed Support

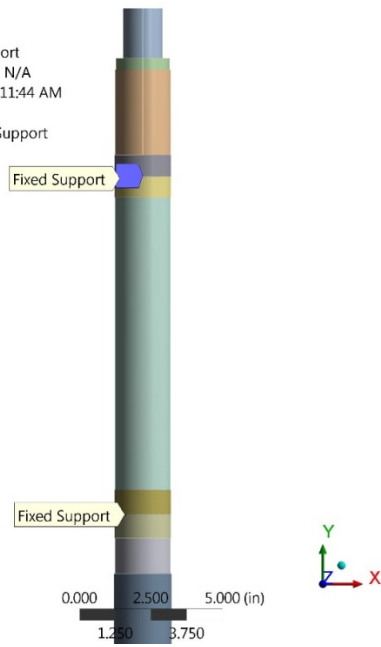


Figure 25. Three-dimensional support.

4.2.3 Analysis Results

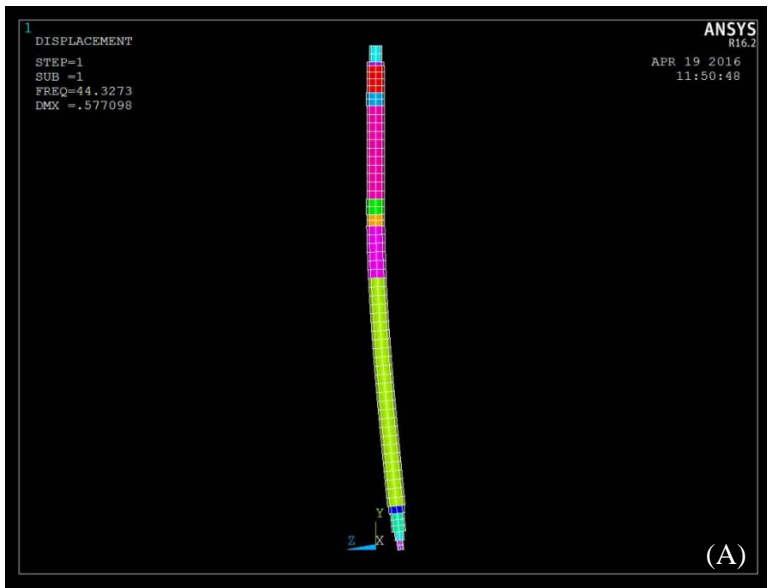
The software program ANSYS [27] was used for the analyses of both models. Modal analysis combined with total deformation was used to determine the natural frequencies of the models and their respective mode shapes.

The natural frequencies of the first ten modes calculated for the beam model and 3-D model are shown in Table 5. The mode shape for each natural frequency is depicted in Figure 26 through Figure 35. Owing to the shaft symmetry, there are two modes at each bending frequency. The figures show that one mode of each pair is bending in the Z-direction and the other pair is bending in the Y-direction. Mode 7 is an axial mode, so there is not a second mode at this frequency.

The two methods produce results with similar mode shapes, and the natural frequencies have a less than 1.5% discrepancy between them.

Table 5. Natural frequencies

Mode	Frequency (Hz)	
	Beam model	3-D model
1	44.327	43.902
2	44.327	44.069
3	266.53	262.48
4	266.53	268.20
5	721.35	711.39
6	721.35	727.80
7	901.82	899.78
8	1362.4	1346.3
9	1362.4	1378.1
10	1418.1	1399.9



A: Modal
 Total Deformation 1
 Type: Total Deformation
 Frequency: 43.902 Hz
 Sweeping Phase: 0. °
 Unit: in
 4/19/2016 11:33 AM

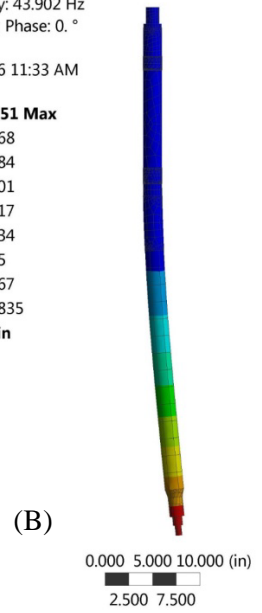
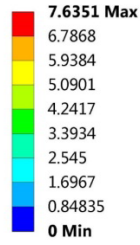


Figure 26. Displacement mode 1: (A) beam model, (B) 3-D model.



Total Deformation 2
 Type: Total Deformation
 Frequency: 44.069 Hz
 Sweeping Phase: 0. °
 Unit: in
 4/19/2016 11:34 AM

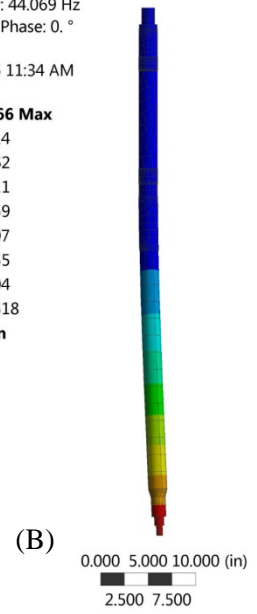
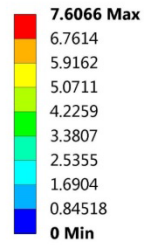


Figure 27. Displacement mode 2: (A) beam model, (B) 3-D model.

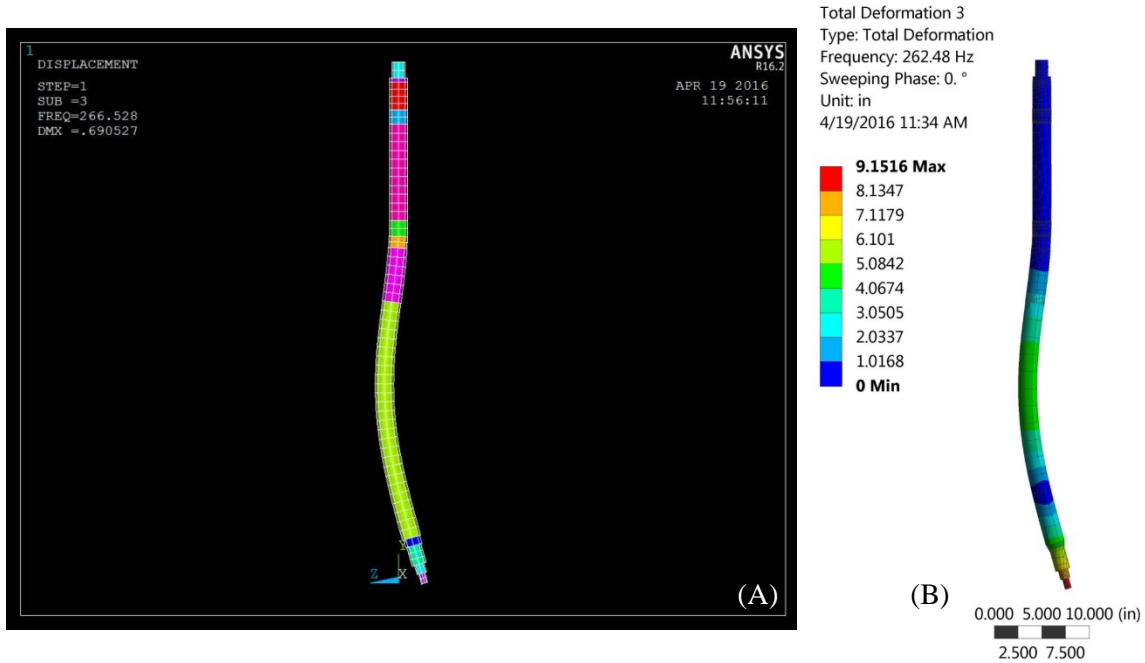


Figure 28. Displacement mode 3: (A) beam model, (B) 3-D model.

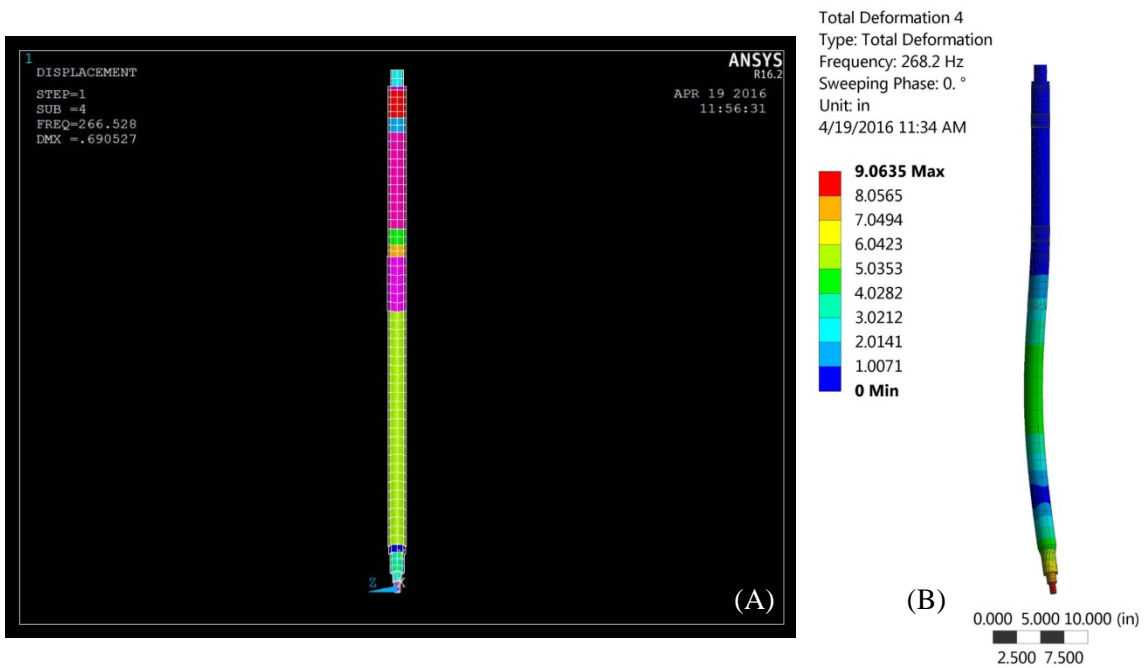


Figure 29. Displacement mode 4: (A) beam model, (B) 3-D model.

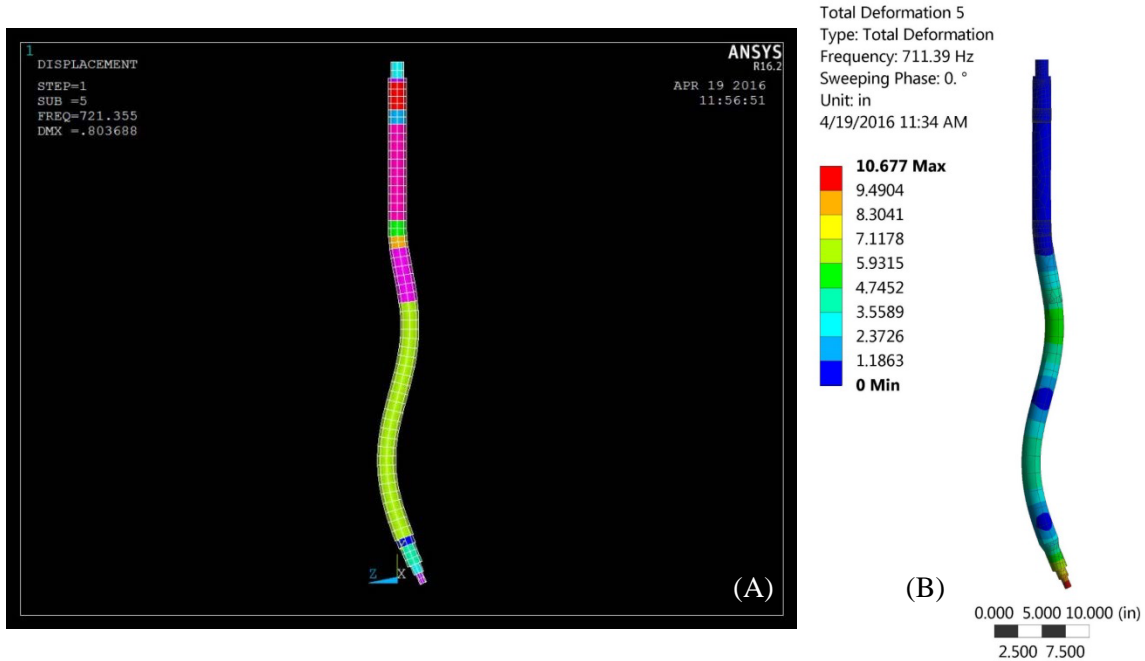


Figure 30. Displacement mode 5: (A) beam model, (B) 3-D model.

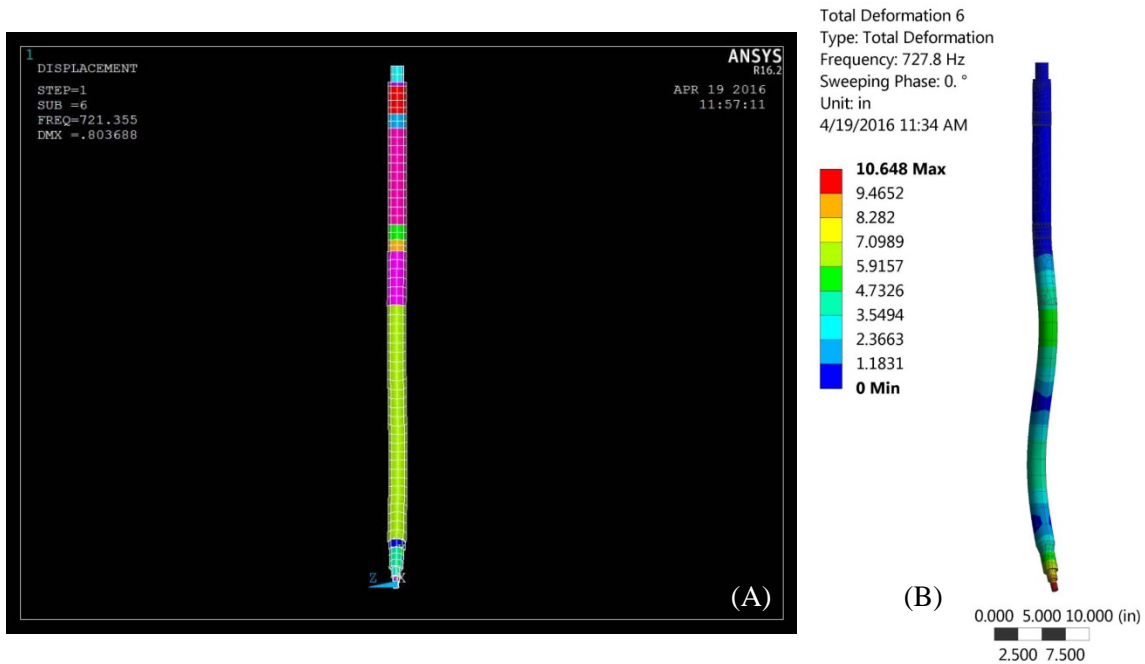


Figure 31. Displacement mode 6: (A) beam model, (B) 3-D model.

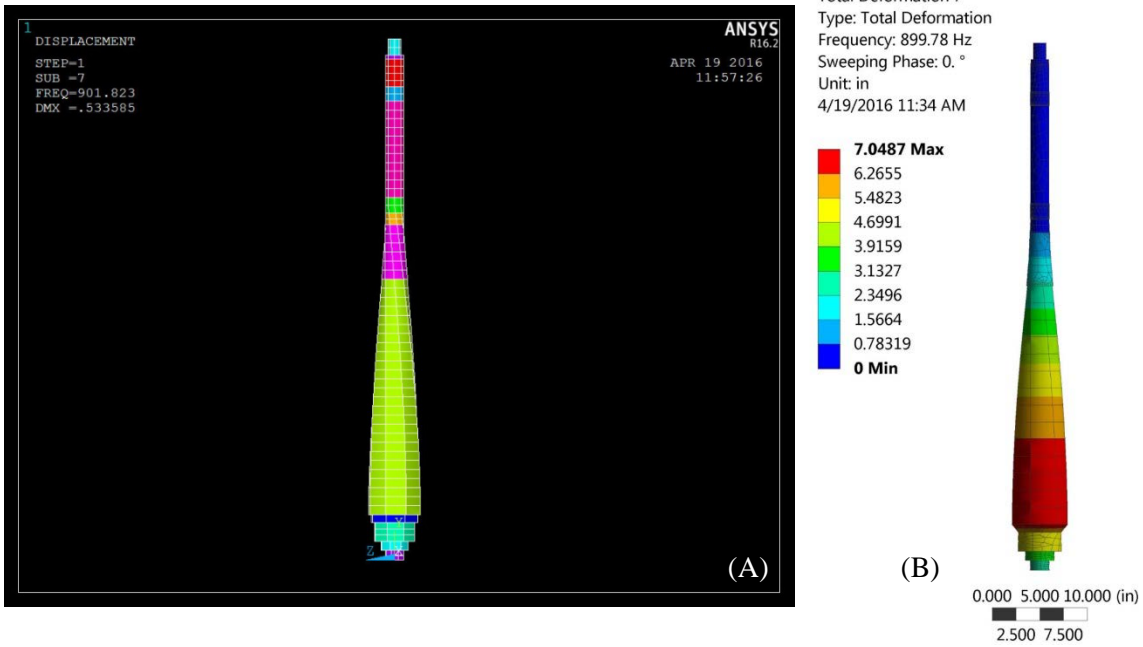


Figure 32. Displacement mode 7: (A) beam model, (B) 3-D model.

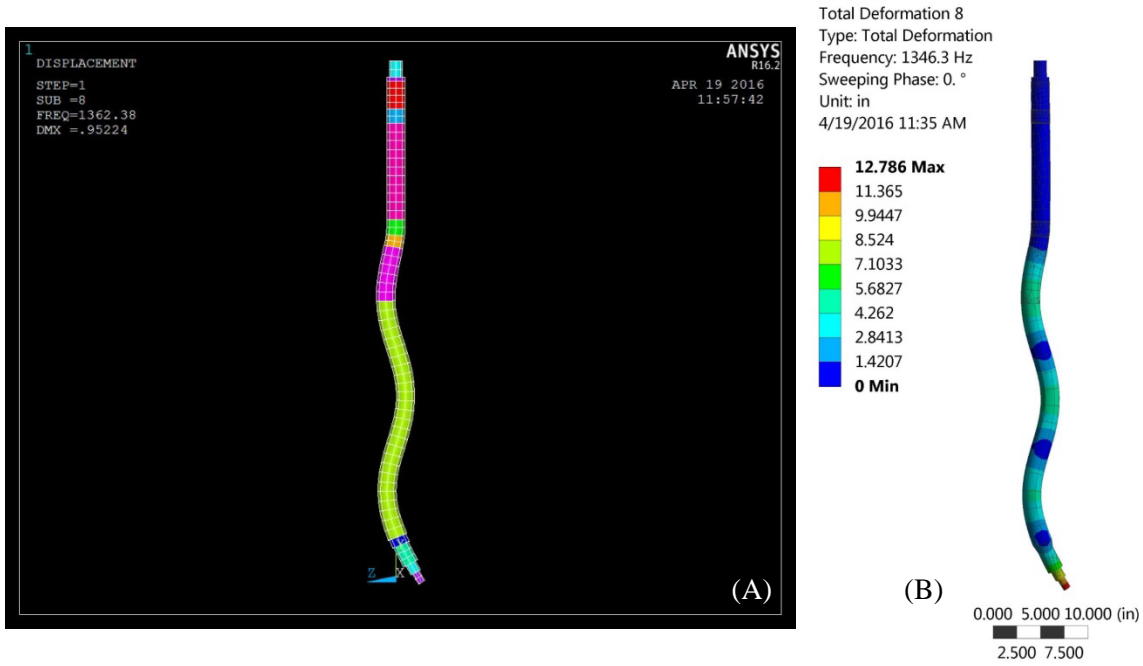


Figure 33. Displacement mode 8: (A) beam model, (B) 3-D model.

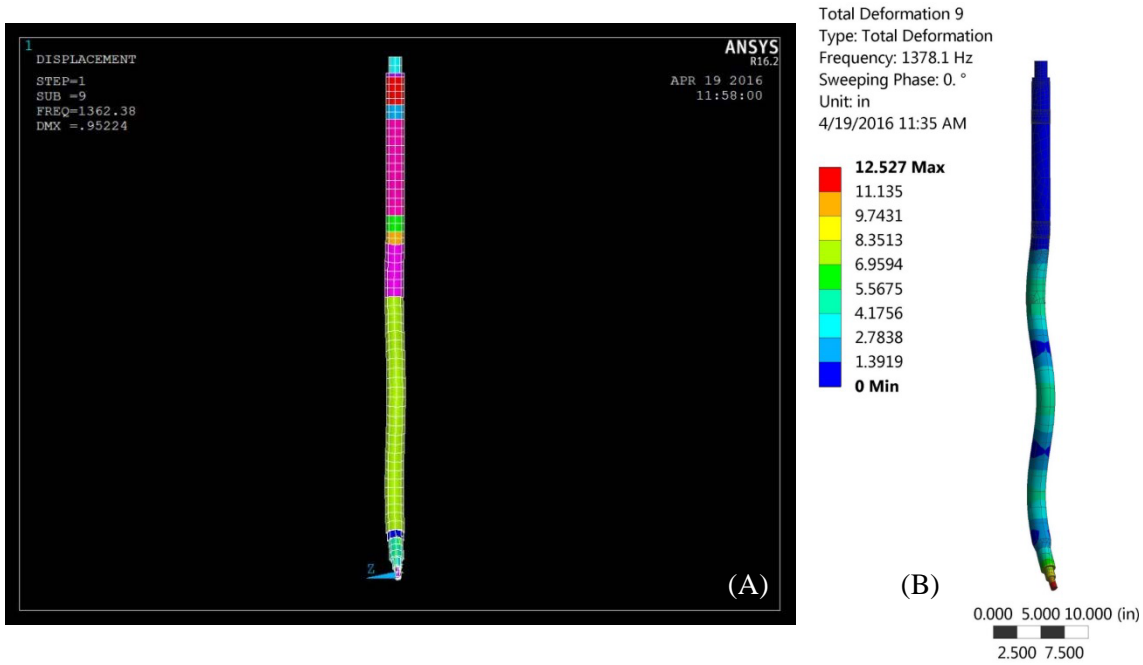


Figure 34. Displacement mode 9: (A) beam model, (B) 3-D model.

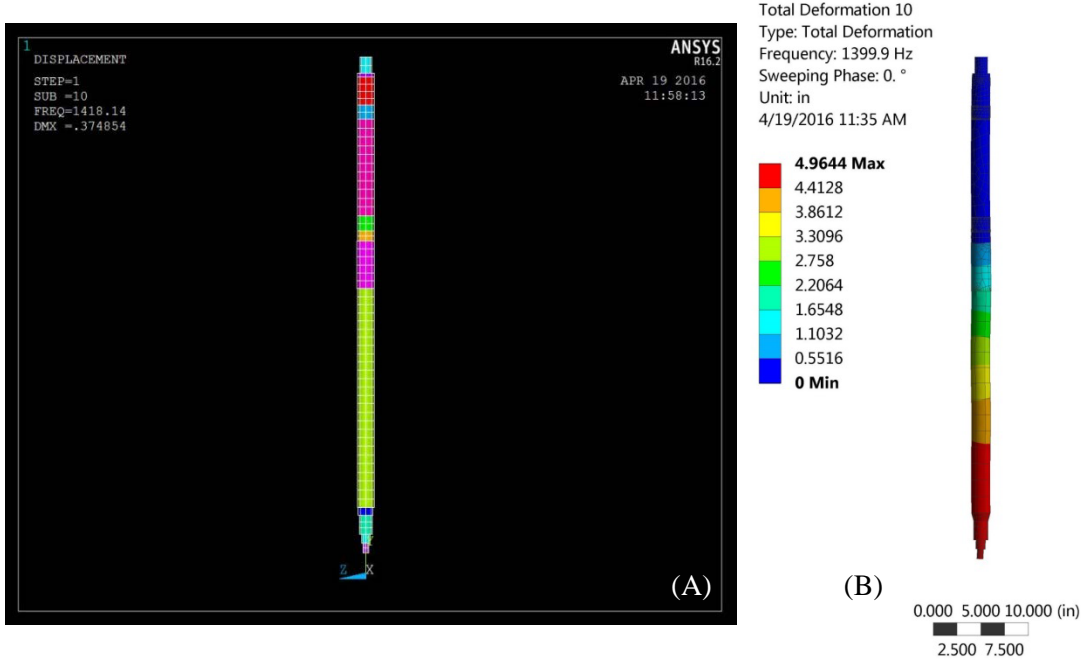


Figure 35. Displacement mode 10: (A) beam model, (B) 3-D model.

4.2.4 Findings and Path Forward

The calculations of the salt pump shaft show that the beam model produces the same natural frequencies and mode shapes as the 3-D model. Therefore, the beam model can be used to model the full system to compare with the impact test data. The beam model will allow for parameter optimization and possible

design changes. The first and second modes correspond to approximately 2,650 rpm. This is within the planned operational range of the LSTL pump (1,100–3,600 rpm).

4.3 COLD SHAKEDOWN TESTING

4.3.1 Initial alignment

During shakedown testing of the loop, under cold gas-filled conditions, substantial vibration was observed during operation of the pump. The alignment of the shaft, bearing housing, and motor were checked. The cause for the excessive vibration was diagnosed as being misalignment of the flexible coupling between the motor and the shaft. This coupling has flange connections at the top and bottom. The coupling design did not include a feature for inherent alignment of the flanged connections during assembly. The “slop” from the clearance between the bolt holes and the bolts resulted in misalignment upon assembly. Vibration was greatly reduced after careful alignment of the coupling during reassembly.

4.3.2 Static Vibration Data

A high-resolution impact test was conducted on the salt pump to calculate the natural frequencies of the system. This characterization can be used to keep the rotational speed of the motor away from the system’s natural frequencies and to validate a finite element model used to optimize the design.

Method

A single-input, single-output roving-hammer impact test was conducted using a force-gauge hammer and an accelerometer mounted onto the motor housing using wax. Nine specific locations were chosen to characterize the system. Because of the symmetric properties of the salt pump and its components, the test was conducted in one direction only. This approach simplifies the system to essentially a vertical column. Each location received four hammer impacts, and the response was averaged for the calculations. In the process of the impact test, frequency response functions (FRF) were calculated to obtain the system’s natural frequencies. The motor operates under 3,600 RPM (60 Hz), so a bandwidth of 200 Hz was chosen to provide ample headroom.

Instrumentation, software, and setup

The following hardware and software were used to perform the impact tests. The pertinent software settings are provided in Table 6. The locations of the hammer impacts and accelerometer are provided in Table 7.

Hardware:

Impact hammer
Accelerometer
M+P VibPilot data acquisition
Laptop

Software:

M+P Smart Office Analyzer

Table 6. Impact test software setup

Parameter	Value
Excitation/hammer	10 mv/lb ICP
Response	100 mv/g
Sample rate	512 Hz
Block size	1024
Delta frequency	0.5 Hz
Acquisition time	2 s
Useful bandwidth	200 Hz
FRF averages	4
Windowing	Force/exponential
force width	10%
Exponential end	10%

FRF – frequency response function

Table 7. Impact test excitation locations

Software name	Description	Location (inches from motor top)
Col.1.x	Motor	0.00
Col.2.x	Top coupling	8.75
Col.3.x	Center coupling	17.25
Col.4.x	Bottom coupling	25.75
Col.5.x	Top bearing	31.75
Col.6.x	Above lower bearing	35.25
Col.7.x	Below lower bearing	41.25
Col.8.x	Center flange	46.25
Col.9.x	Shaft above insulation	50.50
Col.10.x	Impeller housing flange	61.00

Data and Discussion

The natural frequencies based on the calculated FRF data from Figure 36 are tabulated in Table 8. Note that within the FRF data there is a region from 100 Hz to 150 Hz that has a broad response curve with amplitude separation between channels. The largest peak of 116 Hz was chosen as the representative natural frequency for this region.

Table 8. Frequency response from impact test

Frequency number	Natural frequency (Hz)	Corresponding RPM
1	7	420
2	25	1,500
3	44	2,640
4	55	3,300
5	116	6,960
6	154	9,240
7	162	9,720

The planned operation includes steady state motor speeds from 18.3 to 60 Hz. From rest, the motor will go through four natural frequencies and will be very close to the 55 Hz natural frequency during operation at 60 Hz. From Section 4.2, the analysis of the shaft alone also found a natural frequency of 44 Hz.

The natural frequencies, along with their respective modal operational deflection shapes (shown in Figure 37 through Figure 42), can be used to validate future finite element models. Note that the depicted operational deflection shapes are relatively scaled and do not directly represent deflection. The deflection can, however, be calculated given the material properties and dimensions. The deflection shapes do show where the greatest displacement will be and other possibly problematic areas at each natural frequency.

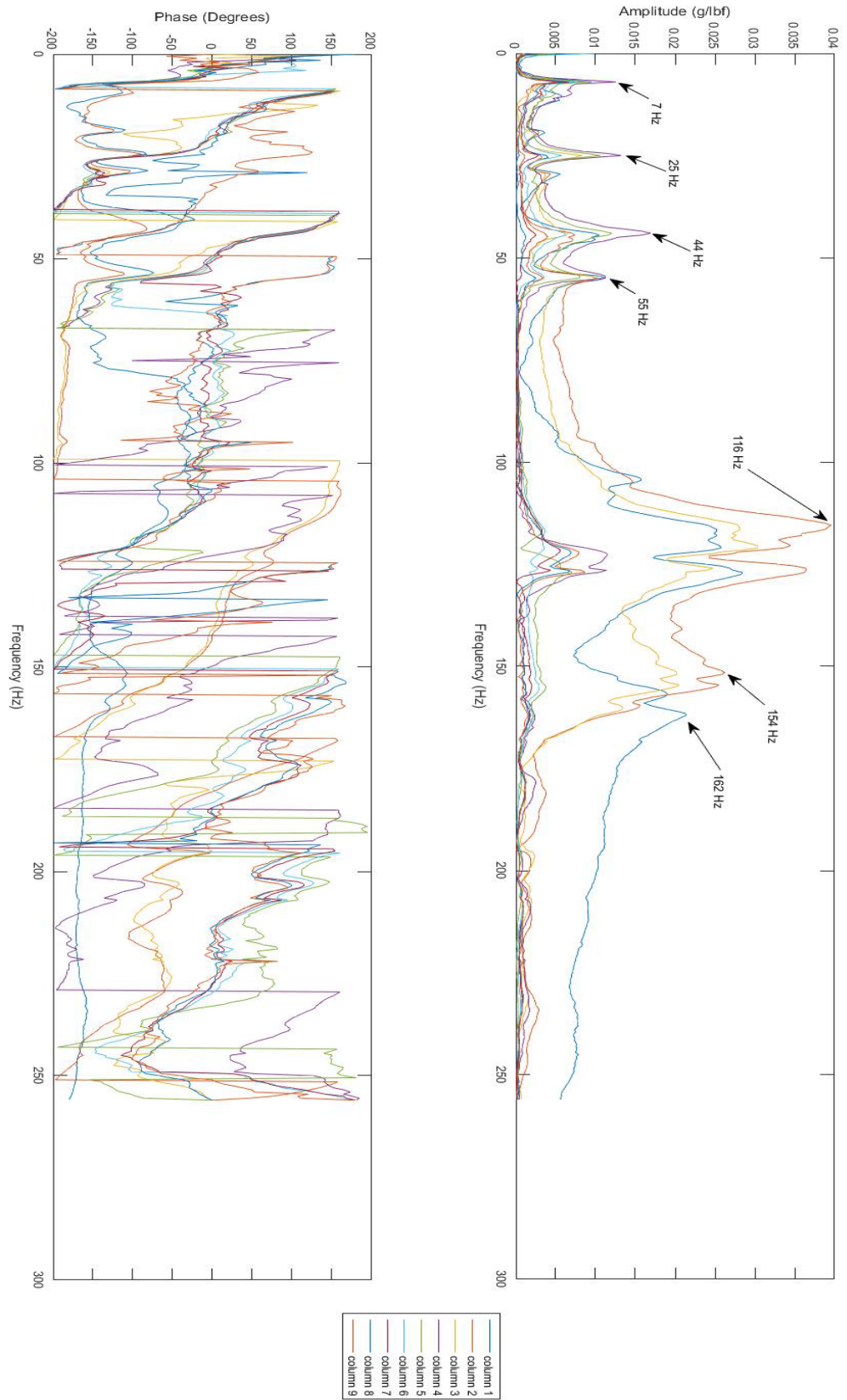


Figure 36. Impact test frequency response function data.

Operational Deflection Shape

f = 7.00 Hz D = 2.84 % ODS Reference Channel 2 [m/N]

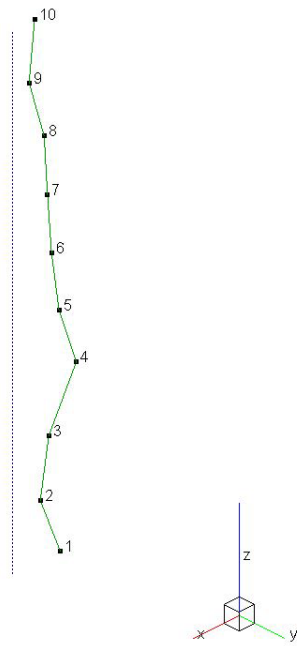


Figure 37. Operational deflection shape at 7 Hz.

Operational Deflection Shape

f = 25.00 Hz D = 2.33 % ODS Reference Channel 2 [m/N]

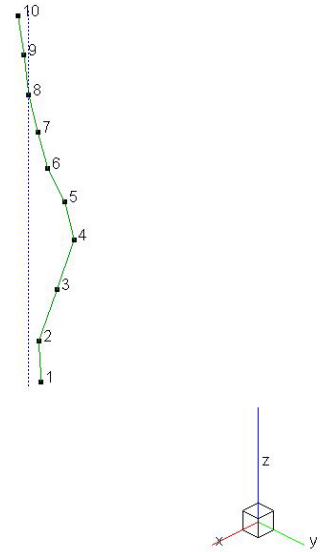


Figure 38. Operational deflection shape at 25 Hz.

Operational Deflection Shape

f = 44.00 Hz D = 2.84 % ODS Reference Channel 2 [m/N]

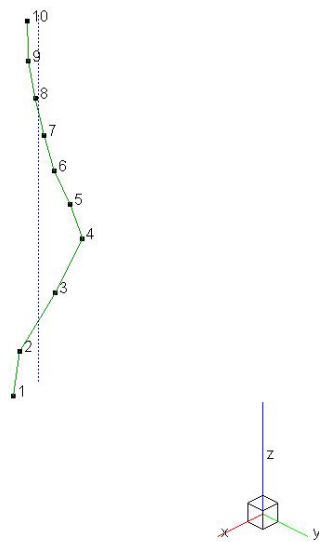


Figure 39. Operational deflection shape at 44 Hz.

Operational Deflection Shape

f = 55.00 Hz D = 1.50 % ODS Reference Channel 2 [m/N]

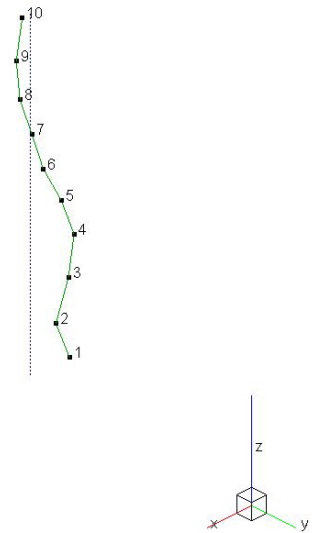
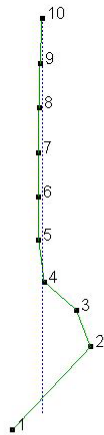


Figure 40. Operational deflection shape at 55 Hz.

Operational Deflection Shape

f = 115.50 Hz D = 2.68 % ODS Reference Channel 2 [m/N]



Operational Deflection Shape

f = 162.00 Hz D = 2.27 % ODS Reference Channel 2 [m/N]

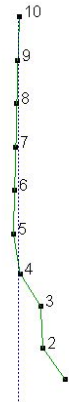


Figure 41. Operational deflection shape at 115 Hz.

Figure 42. Operational deflection shape at 162 Hz.

4.4 FUTURE PLANS

As noted in Section 3.1.2 and Section 3.2.2, a number of pump tests are planned for the future to characterize the performance of the existing pump. Along with this data, plans are to collect additional data in the form of post-test inspection of the impeller. Ultimately, these test data will be used to validate the hydraulic and vibration modeling approaches. These modeling approaches will then be used to design an improved impeller and volute and possibly revise other pump features. Finally, the results from the tests and modeling will inform design guidelines for future salt pump development. A schedule for this research is proposed in Table 9.

The hydraulic, vibration, and thermal characteristics of the pump ultimately influence the structural response of the pump and tank. The structural response is a key design challenge for future pumps, especially as larger pumps are developed. Future work could include developing a structural model of the pump and tank and validating it with appropriate data from the LSTL pump. This validated modeling approach could then be used in future pump designs.

Table 9. Proposed Testing and Model Validation Schedule

		Month											
		1	2	3	4	5	6	7	8	9	10	11	12
Hot testing - Salt Loop*													
System setup	Order & receive equipment	■	■										
	Remove old test section		■										
	Install piping/valve/heat/insulation			■									
	Re-clean system and salt				■								
Existing impeller & volute	Performance testing				■	■	■						
	Post-operation materials test						■						
New impeller & volute	Install new impeller & volute										■		
	Re-clean system and salt											■	
	Performance testing												■
Cold testing - Water loop													
System setup	Order & receive equipment	■	■	■									
	Install & Shakedown		■	■	■								
Existing impeller & volute	Performance testing				■	■	■						
New impeller & volute	Performance testing						**	■	■	■	■		
Model validation and design													
Modeling validation	Hydraulic characteristics (CFD)				■	■	■					■	
	Vibration characteristics				■	■	■					■	
	Comparison of hot and cold testing				■	■	■					■	
New impeller & Volute	Design				**	■	■						
	Fabricate new impeller & volute					**	■	■	■				
Design guidance documentation													
	Quick-look test reports (as needed)				■	■	■	■	■	■	■	■	■
	Final report											■	■

*Dependent upon loop schedule and other testing needs

**Optional testing of preliminary volute and impeller concepts

5. EXAMPLE DESIGN GOALS AND REQUIREMENTS FOR A NEW LSTL-MK2 PUMP

5.1 DESIGN GOALS AND REQUIREMENTS

5.1.1 Goals

Noting that the performance of the existing pump is yet to be determined, the following example goals are proposed for a new pump:

G1: Versatility for use in forced-convection flow loops

G2: Improved efficiency compared with the existing pump

G3: Lower temperatures at the shaft seal and bearings

G4: No gas bubble ingestion/entrainment

The pump would be used for a variety of component tests. Therefore, goal one for the pump is versatility in its operating range and the capability of being modified. The existing pump has large clearances. Goal two is to reduce the clearances to increase efficiency and possibly reduce gas entrainment (although pump efficiency, especially for this size pump, is not required for test loops. Goal three is to lower the temperatures at the bearings and shaft seal; the temperature decrease could be used to either extend bearing and seal life or decrease the overhang length of the shaft. To achieve the latter, modifications such as using a hollow shaft and various cooling gas streams could be undertaken. Goal four for the pump is to eliminate gas/bubble ingestion/entrainment. Gas entrainment could affect testing, such as heat exchanger/heat transfer tests and flow meter testing. Gas entrainment could be eliminated by modifying clearances and inlets and/or including a labyrinth seal.

5.1.2 Requirements

The following are a list of example requirements for a new laboratory-scale salt pump. For a particular application, these requirements would be modified accordingly.

R1: Hydraulic performance: Through varying the speed of the pump, the pump is to produce ____ kg/s at approximately m head to ____ kg/s at approximately m head.

These values would be determined based on the proposed component testing.

R2: Pump lifetime: 2 years of run time

The LSTL, in which the new pump will operate, is primarily constructed of Inconel 600 material. The predicted lifetime of the LSTL, based on the corrosion allowance in FLiNaK at high temperatures, is for 2 years of run time. The pump is expected to operate at high temperature in salt conditions for the 2 year salt operation life of the LSTL.

R3: Radiation tolerance: no radiation tolerance required

The LSTL does not operate in an above-background radiation environment. Therefore, there is no requirement for the pump components (i.e. electronics, insulation, lubricating oils, elastomeric seals) to survive a radiation field.

R4: Gas ingestion: the design of the shaft-casing penetration is to prevent the suction of gas into the pump and limit the spray of salt out of the pump.

Gas entrainment into the pumped flow can impact LSTL test objectives (e.g., heat transfer, ultrasonic flow meter). Gas entrainment should be limited to prevent these effects. A preliminary value of 0.1% is proposed.

R5: Structural integrity/safety: The pump shall be designed, fabricated, and operated following accepted engineering practices to ensure reasonable assurance of safe operation.

Safe operation of the pump is required. The pump structural members and fasteners are to be designed to include a factor of safety margin consistent with accepted engineering practices. Rotating components will be encased in machine guards.

R6: Maintenance: Pump components shall be designed to allow replacement or inspection within 2 days.

The design of the pump is to include reasonable access for maintenance and/or part replacement with respect to research and development efficiency (cost, schedule). Components more likely to need to be replaced, such as the bearings, shaft seal, and motor, should be reasonably replaceable.

R7: Reliability: The pump should be designed to run maintenance-free for the planned lifetime of the pump (2 years).

Reliability is not safety-significant as it is in reactor operation; however, this requirement does affect the cost and timetable for research and development activities. The motor, bearings, seal, and material thicknesses should be designed with sufficient margin to last for the operation life of the pump.

R8: Cost: A budget of \$_____ K for acquisition of a complete assembled pump.

The cost of the pump, including design, fabrication, and installation, will be based on the available resources and the timetable for the planned research. This cost will not include research-related costs such as additional instrumentation and controls, testing, or additional parts.

6. SUMMARY

Progress has been made in a number of areas regarding pump performance characterization and guidelines for salt pump design.

The review of research during the 1950s–1970s on salt pump design, testing, and operational experience highlighted the large amount of work performed in years past (Section 2.1). Researchers gained extensive experience with 14 pump designs totaling over 96 years of operation. Issues such as gas ingestion, gas line plugging, and rubbing were noted and were ultimately overcome. In addition, a number of development pumps were tested. The focused research on key issues, such as seal and bearing performance, was also highlighted. The research was constrained by the materials and manufacturing techniques of that time. However, many of the issues and their development path remain relevant today.

More recently, a pump has been designed, fabricated, and installed in ORNL’s LSTL (Section 2.2). Methods for cold (Section 3.1) and hot (Section 3.2) pump testing were developed, and proposed tests were identified. As of this writing, the LSTL pump has not operated in salt. Only one issue, associated with the alignment of the flexible shaft coupling, has been experienced (Section 4.3.1). In preparation for operation, there was a focused effort on developing models to predict the hydraulic performance of the pump (Section 4.1). This effort explored two different modeling methodologies and predicted pump curves and dynamic pressures experienced in the pump. Also, initial efforts in modeling the vibration performance of the pump explored two different methodologies for modeling the shaft (Section 4.2). Both methodologies performed at a similar level, and the tests identified a number of natural frequencies of the shaft. We may avoid operation at a natural frequency identified as approximately 2,650 rpm. Initial cold-static vibration testing of the pump was performed and identified four natural frequencies within the planned operating range (Section 4.3.2).

The planned pump-focused tests, along with data from the upcoming LSTL heat transfer testing, will be valuable for:

1. validating modeling methodologies for future use in pump design,
2. providing empirical data and experience on the pump performance/issues, and
3. ultimately informing future design guidance for salt pumps.

A preliminary set of design goals and requirements for a future LSTL pump was drafted (Section 5). These goals and requirements will be adjusted in the future based on the salt pump design guidelines developed as this work progresses

7. REFERENCES

1. G. L. Yoder, Jr., et. al., *High-Temperature Fluoride Salt Test Loop*, ORNL/TM-2012/430, Oak Ridge National Laboratory, Dec. 2015.
2. G. L. Yoder, Jr., et. al., “An experimental test facility to support development of the fluoride-salt-cooled high-temperature reactor,” *Annals of Nuclear Energy* **64**, 511–517 (Feb. 2014).
3. E. S. Farris, *Summary of High Temperature, Liquid Metal, Fused Salt Pump Development Work in the ORNL-ANP Project for the Period July 1950-Jan. 1954*, ORNL-CF-54-8-234, Oak Ridge National Laboratory, Aug. 1954.
4. A. P. Fraas and A. W. Savolainen, *Design Report on the Aircraft Reactor Test*, ORNL-2095, Oak Ridge National Laboratory, May 1956.
5. P. G. Smith, *Experience with High-Temperature Centrifugal Pumps in Nuclear Reactors and their Application to Molten-Salt Thermal Breeder Reactors*, ORNL-TM-1993, Oak Ridge National Laboratory, Sept. 1967.
6. W. R. Huntley and P. A. Gnadt, *Design and Operation of a Forced-Circulation Corrosion Test Facility (MSR-FCL-1) Employing Hastelloy N*, ORNL-TM-3863, Oak Ridge National Laboratory, 1974
7. A. N. Smith, *Experience with Sodium Fluoroborate circulation in an MSRE-Scale Facility*, ORNL-TM-3344, Oak Ridge National Laboratory, 1972.
8. W. R. Huntley and M. D. Silverman, *System Design Description of Forced-Convection Molten-Salt Corrosion Loops MSR-FCL-3 and MSR-FCL-4*, ORNL/TM-5540, Oak Ridge National Laboratory, Nov. 1976.
9. W. C. Tunnell, *Seals and Packing Materials for Molten Fluoride Salts*, ORNL-TM-386, Oak Ridge National Laboratory, 1956.
10. R. C. Robertson, *MSRE Design and Operations Report, Part I, Description of Reactor Design*, ORNL-TM-728, Oak Ridge National Laboratory, Jan. 1965.
11. A. G. Grindell, W. F. Boudreau, and H. W. Savage, “Development of centrifugal pumps for operation with liquid metals and molten salts at 1100–1500°F, *Nuclear Science and Engineering* **7**, 83–91 (1960).
12. D. Scott and A. G. Grindell, *Components and Systems Development for Molten-Salt Breeder Reactors*, ORNL-TM-1855, Oak Ridge National Laboratory, June 1967.
13. W. C. Tunnell, *Compatibility Tests of Materials for use in Bearings, Seals, and Valves in Fuse Fluoride Salts at 1200F*, ORNL-2103, Oak Ridge National Laboratory, Sept. 1956.
14. P. G. Smith, “High-temperature molten-salt lubricated hydrodynamic journal bearings,” *ASLE Trans.* **4**, 263–274 (1961).
15. P. G. Smith, *Water Test Development of the Fuel Pump for the MSRE*, ORNL-TM-79, Oak Ridge National Laboratory, Mar. 1962.
16. J. R. Engel, P. N. Haubenreich, and A. Houtzeel, *Spray, Mist, Bubbles, and Foam in the Molten Salt Reactor Experiment*, ORNL-TM-3027, Oak Ridge National Laboratory, June 1970.
17. E. S. Bettis, et al., “The Aircraft Reactor Experiment—Design and construction,” *Nuclear Science and Engineering* **2**, 804–825 (1957).

18. E. S. Bettis, et al., “The Aircraft Reactor Experiment—Operation,” *Nuclear Science and Engineering* **2**, 841–853, 1957.
19. D. Scott, et. al., *A Zero Power Reflector-Moderated Reactor Experiment at Elevated Temperature*, ORNL-2536, Oak Ridge National Laboratory, Aug. 1958.
20. P. N. Haubenreich and J. R. Engel, “Experience with the Molten-Salt Reactor Experiment,” *Nuclear Applications & Technology* **8** (Feb. 1970).
21. J. R. Engel and R. C. Steffy, *Xenon Behavior in the Molten Salt Reactor Experiment*, ORNL-TM-3464, Oak Ridge National Laboratory, Oct. 1971.
22. P. G. Smith, *Development of Fuel- and Coolant-Salt Centrifugal Pumps for the Molten-Salt Reactor Experiment*, ORNL-TM-2987, Oak Ridge National Laboratory, Oct. 1970.
23. CFD Module- User’s Guide, “Theory for the Rotating Machinery Interfaces,” COMSOL Version 5.2, 2016. Available from www.comsol.com.
24. J. Richard, D. Wang, G. Yoder, J. Carbajo, D. Williams, B. Forget, and C. Forsberg, “Implementation of Liquid Salt Working Fluids into TRACE,” Paper 14214 in *Proceeding of ICAPP 2014*, Charlotte, North Carolina, USA, April 6–9, 2014, American Nuclear Society.
25. V. Lobanoff and R. Ross, *Centrifugal Pumps—Design and Application*, 2nd ed., Woburn, Mass., Butterworth-Heinemann, 1992.
26. J. G. Sessler and V. Weiss, *Aerospace Structural Metals Handbook*, 4th revision, Syracuse University, 1967.
27. ANSYS Mechanical, Release 16.2, Ozen Engineering, August 2015.